

# Extremes in East African hydroclimate and links to Indo-Pacific variability on interannual to decadal timescales

Caroline C. Ummenhofer<sup>1</sup> · Marco Kulüke<sup>2</sup> · Jessica E. Tierney<sup>3</sup>

Received: 26 September 2016 / Accepted: 4 July 2017 / Published online: 11 July 2017  
© Springer-Verlag GmbH Germany 2017

**Abstract** East African hydroclimate exhibits considerable variability across a range of timescales, with implications for its population that depends on the region's two rainy seasons. Recent work demonstrated that current state-of-the-art climate models consistently underestimate the long rains in boreal spring over the Horn of Africa while overestimating the short rains in autumn. This inability to represent the seasonal cycle makes it problematic for climate models to project changes in East African precipitation. Here we consider whether this bias also has implications for understanding interannual and decadal variability in the East African long and short rains. Using a consistent framework with an unforced multi-century global coupled climate model simulation, the role of Indo-Pacific variability for East African rainfall is compared across timescales and related to observations. The dominant driver of East African rainfall anomalies critically depends on the timescale under consideration: Interannual variations in East African hydroclimate coincide with significant sea surface temperature (SST) anomalies across the Indo-Pacific, including those associated with the El Niño-Southern Oscillation (ENSO) in the eastern Pacific, and are linked to changes in the Walker circulation, regional winds and vertical velocities over East Africa. Prolonged drought/pluvial

periods in contrast exhibit anomalous SST predominantly in the Indian Ocean and Indo-Pacific warm pool (IPWP) region, while eastern Pacific anomalies are insignificant. We assessed dominant frequencies in Indo-Pacific SST and found the eastern equatorial Pacific dominated by higher-frequency variability in the ENSO band, while the tropical Indian Ocean and IPWP exhibit lower-frequency variability beyond 10 years. This is consistent with the different contribution to regional precipitation anomalies for the eastern Pacific versus Indian Ocean and IPWP on interannual and decadal timescales, respectively. In the model, the dominant low-frequency signal seen in the observations in the Indo-Pacific is not well-represented as it instead exhibits overly strong variability on subdecadal timescales. The overly strong ENSO-teleconnection likely contributes to the overestimated role of the short rains in the seasonal cycle in the model compared to observations.

## 1 Introduction

Variations in East African hydroclimate across a range of timescales have the potential to greatly affect the livelihood of the region's population. Recurring drought conditions across East Africa in recent decades, such as those in 1998, 2000, 2005, and almost continuously post-2008 especially during 2009–2011 (Nicholson 2014, 2016a), have redoubled research efforts to elucidate their origin. Droughts in the Horn of Africa have been linked to Indo-Pacific sea surface temperatures (SST; Funk et al. 2014; Hoell and Funk 2014; Funk and Hoell 2015; Hoell et al. 2017), partially driven by anthropogenic aerosol emissions (Rowell et al. 2015), changes in the tropical Pacific Ocean (Lyon and DeWitt 2012; Lyon 2014), in particular changing zonal Pacific SST gradients (Liebmann et al. 2014), a

Revised for Climate Dynamics.

✉ Caroline C. Ummenhofer  
cummehofer@whoi.edu

<sup>1</sup> Department of Physical Oceanography, Woods Hole Oceanographic Institution, Woods Hole, MA, USA

<sup>2</sup> Department of Earth Sciences, University of Hamburg, Hamburg, Germany

<sup>3</sup> Department of Geosciences, University of Arizona, Tucson, AZ, USA

westward extension of the Indo-Pacific warm pool (IPWP) and a strengthening of the Walker circulation (Williams and Funk 2011) leading to enhanced upper-level easterlies over East Africa (Liebmann et al. 2017), a warming Indian Ocean (Funk et al. 2008; Williams et al. 2012), and anomalous subsidence over East Africa associated with unusually strong equatorial westerlies over the Indian Ocean (Hastenrath et al. 2007, 2010), amongst others.

Anomalously dry and wet conditions in East Africa have been attributed to different climatic drivers; some of the apparent disagreement amongst studies in that regard is likely due to differences in study design: this arises from addressing different seasons or timescales (interannual versus decadal variability), using different data sets (especially pronounced in this data-sparse region), and varying analysis periods due to the non-stationarity of the climatic drivers in the region (e.g., Nicholson 2015, 2017). It is therefore of interest to investigate these aspects systematically in a consistent framework, such as that provided by an unforced multi-century simulation with a global coupled climate model. Here we use a 1300-year pre-industrial control simulation from the National Center for Atmospheric Research (NCAR) Community Earth System Model (CESM) to compare the role of Indo-Pacific variability on East African rainfall on interannual and decadal timescales.

East Africa exhibits much drier conditions in the annual mean sense compared to other tropical land areas, with a distinct bimodal rainfall distribution (Yang et al. 2015). Nicholson (2016b) linked the region's aridity to the Turkana low-level jet, strongest during the June–September dry season, that suppresses rainfall, with the region's orography also playing a role (Christensen et al. 2013). Rainfall across the Horn of Africa is characterised by the semi-annual passage of the Intertropical Convergence Zone (ITCZ), which results in two rainy seasons in the region: the so-called “long rains” during March–May (MAM) and the “short rains” during September–November (SON). Investigating atmospheric convective stability over the region, Yang et al. (2015) attributed these distinctive seasonal features to the ventilation mechanism: the atmosphere over East Africa is convectively stable year-round due to the import of low surface moist energy from the relatively cool Indian Ocean; the two rainy seasons represent the exception when SST in the western Indian Ocean rise and less stable air is transported onto East Africa. Using idealised atmospheric general circulation model (AGCM) experiments, Ummenhofer et al. (2009b) assessed the role of Indian Ocean SST during enhanced East African short rains. They found extreme short rains to be primarily due to increased onshore moisture flux convergence driven by local warm SST in the western Indian Ocean, rather than a strengthened zonal SST gradient across the equatorial Indian Ocean associated with the Indian Ocean Dipole (IOD; Saji et al. 1999; Webster

et al. 1999; Black et al. 2003). Related to this, recent warming trends in the western Indian Ocean may be responsible for increasingly wetter short rain seasons (e.g., Liebmann et al. 2014).

On interannual timescales, East African rainfall variability has been associated with Atlantic variability (Camberlin and Okoola 2003; Williams et al. 2012), the El Niño–Southern Oscillation (ENSO; e.g., Janowiak 1988; Ogallo 1988; Mutai et al. 1998; Reason et al. 2000; Giannini et al. 2008; Parhi et al. 2016), the IOD (e.g., Saji et al. 1999; Webster et al. 1999; Black et al. 2003; Manatsa et al. 2012; Manatsa and Behera 2013), zonal equatorial easterlies (Hastenrath et al. 2004), the Mascarene High (Manatsa et al. 2014), and the Southern Annular Mode (Manatsa et al. 2016). Links between East African rainfall variability and ENSO are especially pronounced later in the year (e.g., Janowiak 1988; Ogallo 1988; Mutai et al. 1998; Reason et al. 2000). The question has been raised whether these impacts are a direct response to ENSO-forcing, or more the result of an indirect effect through ENSO's influence on Indian Ocean SST (Goddard and Graham 1999; Latif et al. 1999; Black et al. 2003). Parhi et al. (2016) found the East African short rains to be impacted by ENSO during its mature phase through enhancing Indian Ocean surface warming, leading to increased column water vapour content and higher atmospheric vertical instability across the region. Large-scale variability across the broader Indo-Pacific thus likely plays a role, though the relative contributions from the Pacific and Indian Ocean, as well as their co-variability, vary on decadal timescales.

Investigating interannual variability of the onset and demise of the East Africa long rains, Camberlin and Okoola (2003) found that both Atlantic and Indian Ocean SST were important: a delayed onset of the long rains was associated with warm SST in the South Atlantic and cool SST in the Indian Ocean, leading to enhanced equatorial easterlies and divergent flow over East Africa; such a configuration resulted in a westward displacement of the ITCZ, delaying the onset of the long rains (Camberlin and Okoola 2003). Anomalous warm Indian Ocean SST, often associated with the positive phase of the IOD (Saji et al. 1999; Webster et al. 1999), result in enhanced low-level easterly moisture transport and convergence over East Africa (Ummenhofer et al. 2009b) or a weakening of the westerly flow that transports moisture away from the region over the northern Indian Ocean (Black et al. 2003). The strength of the central Indian Ocean equatorial surface winds also exhibits strong control on East African climate (Hastenrath et al. 2004): short rains are deficient when development of the zonal circulation cell over the Indian Ocean is weak in response to anomalously cool SST in the western Indian Ocean. Central Indian Ocean equatorial winds thus have been proposed as a useful predictor of East African rainfall

(Hastenrath et al. 2004). Funk et al. (2014) instead used two SST indices based on the western Pacific SST gradient and central Indian Ocean SST as predictor for boreal spring rainfall, capturing most major drought events in recent years. Analysing the potential predictability of SST-forced East African rainfall in AGCM simulations, Bahaga et al. (2015) found the IOD to play a dominant role for predicting interannual variability compared to ENSO. In contrast, low-frequency variations in prediction skill after the climate shift in the mid-1970s was thought to be due to ENSO interfering with the Indian Ocean's influence (Bahaga et al. 2015).

Investigating East African rainfall post-1998, Nicholson (2016a) found droughts to be more frequent and persistent after 2005 compared to the earlier period, consistent with a decline in total water storage in the Horn of Africa between 2002 and 2010 (Omondi et al. 2014); equally severe droughts were also encountered in the 1950s and 1970s and an extensive multi-decadal drought in the early 19th century (Nicholson et al. 2012). Using a 139-year precipitation record, Nicholson (2015) evaluated the time-dependence of the impact of ENSO, IOD, and equatorial zonal winds in the central Indian Ocean for East African short rains and found marked variations on decadal timescales: zonal winds exhibited the most consistent link, compared to ENSO and IOD, especially pronounced during wet years. Extremely wet conditions were associated with several of these drivers acting in concert, while drought conditions had more varied causes (Nicholson 2015, 2017).

Decadal changes in the strength of the Walker circulation are intimately tied to the strength of ENSO's influence on East Africa: a strong Walker cell over the Pacific and a weak one over the Indian Ocean during 1920–1960 was associated with strong links to ENSO, overall drier conditions, and suppressed interannual variability in the East African short rains. When the Pacific Walker cell weakened and the Indian Ocean one strengthened post-1961, the short rains became more variable and wetter (Nicholson 2015). Similarly, Manatsa and Behera (2013) described an epochal strengthening in the relationship between the IOD and East African rainfall post-1961, with 73% of short rain variability in East Africa explained by the IOD, up from 50% in previous decades. After 1997, this increased further to 82%, explaining spatially coherent events across the region and frequent rainfall extremes (Manatsa and Behera 2013). Awange et al. (2014) found variability in water storage over the Nile Basin to be significantly associated with the IOD during their study period 2002–2011. The effect of Indian Ocean SST on East African rainfall is most pronounced during the short rains, though Williams and Funk (2011) argued that warming Indian Ocean SST in recent decades were also associated with reduced long rains for the March–June season in Ethiopia and Kenya.

Investigating decadal trends in East African rainfall, Ongoma and Chen (2016) found a long-term decrease since the 1950s over the region 35°–40°E, 5°N–4°S; largest negative annual trends were incurred during the 1960s, while during the 1990s and 2000s drying was especially pronounced during the long rain season (e.g., Nicholson 2017, and references therein). The latter is of particular concern as droughts during the long rains affect crops and livestock across the region (e.g., Ongoma and Chen 2016; Vrieling et al. 2016). Investigating recent changes in Horn of Africa precipitation in observations and SST-forced AGCM simulations, Liebmann et al. (2014) found the MAM rainy season to have become drier and the October–December months wetter since 1979; they linked the former to an increased zonal SST gradient between the Maritime Continent and the central Pacific, while the latter was associated with warming in the western Indian Ocean. Williams et al. (2012) also found East Africa to be increasingly influenced by the southern tropical Indian Ocean since the 1980s, which led to convergence of dry air over East Africa, reducing moisture advection from the Congo Basin and thus lowering convection and rainfall locally. Vigaud et al. (2017) suggested that a more frequent dry regime in May since 1998–99, associated with an earlier onset of the monsoon and Somali jet, could account for a recent abrupt shift observed in East African long rains. They related this shift to off-equatorial warming in the western Pacific modulating the long rains on multi-decadal timescales. Similarly, Lyon (2014) attributed more frequent MAM droughts in East Africa post-1998 to multi-decadal natural variability in the tropical Pacific. In contrast, Hoell et al. (2017) suggested that human-induced changes in tropical SST exacerbated the effect of natural Pacific decadal variability, enhancing East African drying during the long rain season. Tierney et al. (2015) showed that the recent drying in the Horn of Africa was unusual in the context of the last 2000 years and likely related to warming temperatures associated with rising greenhouse gases.

For 21st Century projections, Conway et al. (2007) found no clear trend in annual East African rainfall, but an indication of decreased MAM and increased SON values based on six different Coupled Model Intercomparison Project phase 3 (CMIP3) models. Shongwe et al. (2011) also described increases in the mean and extreme precipitation during the short rains based on 12 CMIP3 models. This was associated with a positive IOD-like warming projected for the 21st Century, resulting in enhanced moisture convergence over East Africa due to a weakened descending branch of the Walker cell (Christensen et al. 2013). Cook and Vizzy (2013) used a regional climate model forced with a medium-emissions scenario based on a six-member ensemble of CMIP5 models to investigate changes in East African rainy seasons: the projections indicated shorter and

drier long rains across East Africa due to strong warming over the Sahara and anomalous dry anticyclonic flow from the northern Arabian Sea. This was also consistent with projected increases in dry days over East Africa (Vizy and Cook 2012), while the short rains were prolonged due to a northeastward shift in the South Indian convergence zone (Cook and Vizy 2013).

Recent work demonstrated that current state-of-the-art climate models consistently overestimate the short rains, while underestimating the long rains over the Horn of Africa (Tierney et al. 2015; Yang et al. 2014). According to Yang et al. (2014), the CMIP5 historical simulations therefore erroneously indicate a slight wettening trend for the long rains in the 20th Century in response to the radiatively forced change. In contrast, the atmospheric model intercomparison project (AMIP) experiments with observed SST forcing exhibit East African precipitation trends consistent with observations and also have a more realistic seasonal cycle. Tierney et al. (2015) found future projections were unrealistically dominated by a weakening of the Walker circulation predicting increasingly wetter conditions for East Africa, while the observations and palaeoclimate records suggest extensive drying. This inability to represent the seasonal cycle makes it problematic for current state-of-the-art climate models to project changes in precipitation for East Africa. Here we explore whether this also has implications for the model's representation of interannual and decadal variability in East African precipitation during the long and short rain seasons.

The remainder of the paper is structured as follows: Section 2 describes the observational and reanalysis products and climate model simulation. In Section 3, the simulated characteristics of East African hydroclimate are compared to observations. Links between East African hydroclimatic extremes and Indo-Pacific climate anomalies are detailed in Section 4. Section 5 assesses spectral properties of SST of relevance for East Africa in the Indian and Pacific Ocean basins, respectively. Our main findings are summarised in Section 6.

## 2 Data sets and model

### 2.1 Observational and reanalysis products

A series of monthly global gridded observational and reanalysis products were used to assess the representation of the model's climate conditions. At 2.5° horizontal resolution, these include the National Centers for Environmental Prediction (NCEP)/National Center for Atmospheric Research (NCAR) reanalysis (NNR; 1948–present; Kalnay et al. 1996; Kistler et al. 2001) and the 20th Century reanalysis (20CR; 1871–2011; Compo et al. 2011); SST at 1°

horizontal resolution from the UK Hadley Centre HadISST (1870–present; Rayner et al. 2003); and precipitation at 0.5° horizontal resolution from the Global Precipitation Climatology Centre (GPCC; version 6; 1901–2010; Schneider et al. 2013). Quantifying uncertainties in precipitation is especially difficult over Africa due to the poor distribution of the rain gauge network. Awange et al. (2016) compared six newly available satellite-based precipitation products over the Horn of Africa and found them to be consistent with GPCC for the overlapping study period 2003–2010. Here, the common analysis period was taken as 1901–2010, though results were repeated for the more recent period post-1957 with improved data coverage. Given the robustness of the results, we only show analyses for the longer period 1901–2010.

### 2.2 Climate model

We make use of output from the Community Earth System Model (CESM), a fully coupled state-of-the-art global community climate model developed by NCAR, which is part of CMIP5. The atmospheric component of the model, the Community Atmosphere Model version 4 (CAM4), provides considerable improvements to the earlier version of the model, such as changes in the deep convection parameterisation through subgrid-scale convective momentum transports (Gregory et al. 1997; Richter and Rasch 2008), which improved subtropical westerly biases, the excessive mid-latitude jet in the Southern Hemisphere, and representation of ENSO. The finite volume scheme was used for the dynamical core component due to its superior transport properties and new horizontal grid discretisations (1.9° by 2.5° and 0.9° by 1.25°) were made for improved computational processing (Neale et al. 2012). For further information on the mean climate of CAM4 in fully coupled simulations, see Neale et al. (2013).

The ocean component of CESM consists of the Los Alamos National Laboratory Parallel Ocean Program Version 2 [POP2; (Smith et al. 2010)] and the Community Sea Ice Model (Briegleb et al. 2004). The horizontal resolution is roughly 1° with refined meridional spacing in the tropics and 60 vertical levels with improved resolution in the upper 160 m with uniform 10-m resolution. Some significant efforts for the improved subgrid-scale parameterisations have been made in recent years for POP2, as summarised in detail by Smith et al. (2010) and Danabasoglu et al. (2012). Some of the relevant updates to the topic of this study are the inclusion of space-time dependent thickness and isopycnal diffusivity (Danabasoglu and Marshall 2007), anisotropic horizontal viscosity and diffusivity (Jochum and Potemra 2008; Jochum 2009), the parameterisations for mesoscale eddy flux (Danabasoglu et al. 2008), and sub-mesoscale eddies (Fox-Kemper et al. 2011).



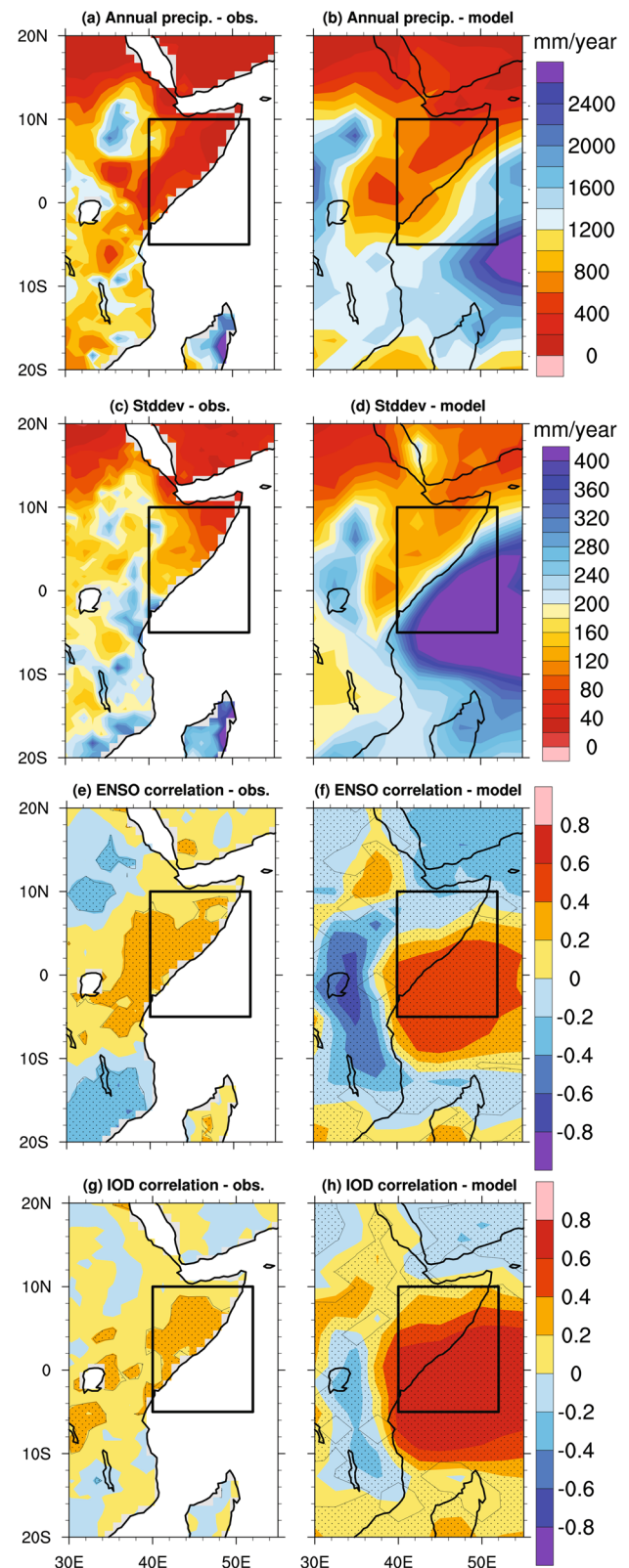
**Fig. 1** Regional precipitation and correlations with ENSO and IOD for (left) observations and (right) model, all for annual values (averaged for September–August months): **a, b** total precipitation (mm/year); **c, d** standard deviation of precipitation (mm/year); **e, f** correlation coefficient between the Niño3.4 index and precipitation; and **g, h** correlation coefficient between the Dipole Mode Index and precipitation. The *black box* indicates the region used for time-series analysis. Stippling indicates significant correlations at the 95% confidence level

### 3 East African hydroclimate

#### 3.1 Mean, correlation, and seasonal cycle

Characteristics of East African precipitation in Fig. 1 highlight how mean rainfall, its variability, and important teleconnections compare between observations and the model. Long-term mean annual precipitation across the region is characterised by rainfall amounts of 800–1400 mm/year for much of the region, with drier conditions of only 200–400 mm/year over the Horn of Africa (Fig. 1a, b). While the model captures reduced precipitation in the Horn region, the precipitation minimum of less than 200 mm/year seen at the tip of the Horn in observations is too wet in the model. The model simulates the enhanced precipitation over the Ethiopian Highlands, but the high-rainfall region extends too far west and south compared to observations. Year-to-year variability of annual precipitation is low for the Horn of Africa, in particular near the tip of the Horn, a feature well-represented by the model (Fig. 1c, d). The model overestimates precipitation variability further inland, though.

It is well-known that East African precipitation is affected by Indo-Pacific variability associated with ENSO (e.g., Janowiak 1988; Ogallo 1988; Mutai et al. 1998; Indeje et al. 2000; Lyon and DeWitt 2012) and the IOD (e.g., Goddard and Graham 1999; Saji et al. 1999; Webster et al. 1999; Black et al. 2003; Behera et al. 2005; Hastenrath 2007; Ummenhofer et al. 2009b; Manatsa et al. 2012; Manatsa and Behera 2013). To take into account the seasonal evolution of ENSO and IOD events, the precipitation time-series used in Fig. 1 has been shifted to cover the September to August months. The correlation between annual precipitation and the Niño3.4 index as the spatially averaged SST in the central equatorial Pacific (5°N–5°S, 170°–120°W) and the Dipole Mode Index (DMI; Saji et al. 1999) is shown in Fig. 1e–h. Precipitation in the Horn of Africa region in observations is positively correlated with ENSO, with higher correlations for the latitude band 5°N–5°S and along the coast, while negative anomalies are seen south of 10°S and north of 10°N (Fig. 1e). The broad features of the ENSO-precipitation correlation are captured by the model (Fig. 1f), though the area of high correlations is much stronger and more restricted to the coast and the



southern Horn compared to observations. East African precipitation in observations and the model is also positively correlated with the IOD, though the correlation coefficient

over the Horn region is overly strong in the model (Fig. 1g, h).

To better understand hydroclimatic variations in East Africa, precipitation is averaged over the land-points within the region 10°N–5°S, 40°–52°E as delimited by the box in Fig. 1 that includes Somalia, parts of Ethiopia and Kenya. The spatial extent of the region is determined by being an area of interest that has recently experienced severe drought conditions (e.g., Nicholson 2014) and its hydroclimatic features are simulated by the model. In the comparison between observations and simulated East African hydroclimate, the limited number of high-quality records that are available for the gridded observational product across the region should be kept in mind.

The seasonal cycle of the precipitation time-series, spatially averaged across the land-points in the Horn of Africa region (cf. spatial extent highlighted in Fig. 1) is shown for the observations and model in Fig. 2. The seasonal cycle highlights the two rainy season characteristics of East African hydroclimate in observations: the long rains during MAM and the short rains during SON (Fig. 2a). The large year-to-year variability during the rainy seasons and less so for the intervening drier months is also apparent. In the model, the seasonal cycle of the total rainfall overemphasises the short rains with a mean ranging from 70–120 mm/month in SON, compared to a mean of 30–60 mm/month in the observations (Fig. 2a, b). In contrast, the model long rains are considerably underestimated in the model. Given the importance of the Turkana low-level jet in suppressing rainfall (Nicholson 2016b), a bias in the jet in the model could contribute to biases in the short and long rains. The

climatological MAM winds at the 850hPa level in the model over the entry region of the Turkana jet are somewhat stronger and exhibit a northerly bias compared to observations: i.e., the jet is angled from the southeast in the observations, rather than directly from the east in the model (figure not shown). During SON, the alignment of the Turkana jet over the entry region is well-represented in the model, though the jet is weaker than in observations, which could contribute to the positive bias in the short rains in the model.

The bimodal rainfall distribution of the seasonal cycle in observations is better reflected in the convective precipitation in the model (Fig. 2c), though the model peak in the long rains is shifted towards May, compared to April in the observations. The large-scale precipitation in the model (figure not shown) exhibits a small contribution to the total rainfall, more or less uniform throughout the year, a bias common to climate models that rain too frequently in the 1–10 mm/day category (e.g., Dai 2006, and references therein). For the remainder of the study, we therefore focus our analyses on the convective precipitation in the model which has a more realistic seasonal cycle and precipitation amounts for the Horn of Africa region of interest here.

### 3.2 Time-series and extremes

The precipitation time-series for the Horn of Africa region are given for the MAM and SON season in the observations and model in Fig. 3. Highlighted are individual seasons with extreme hydroclimatic conditions, defined as those with the highest/lowest 10% of seasonal precipitation

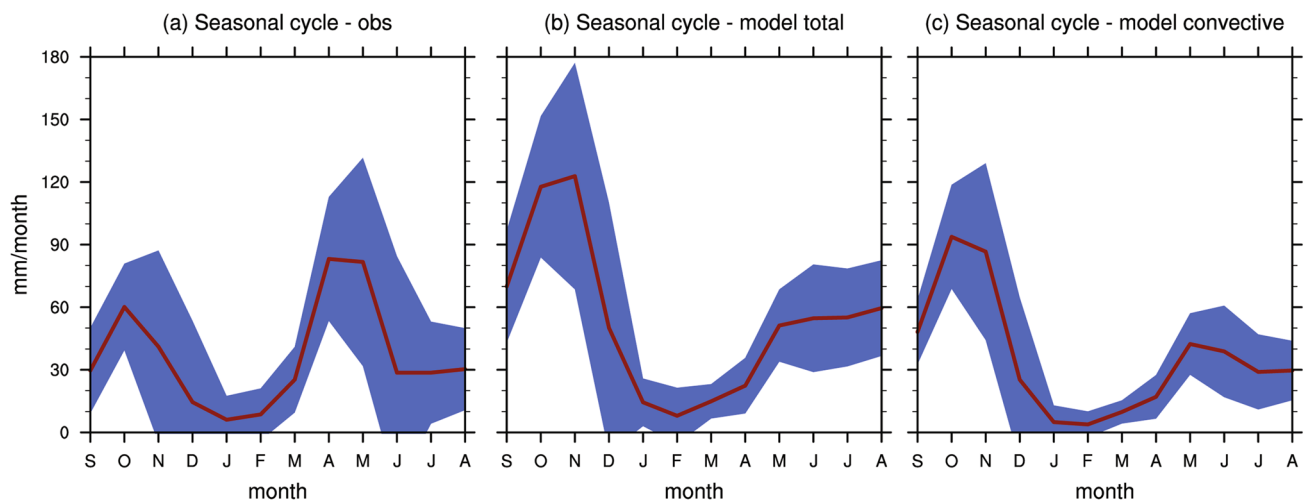


**Fig. 2** Seasonal cycle in precipitation (mm/month) over East Africa (cf. land-points in the box in Fig. 1) for **a** observations, **b** model total precipitation, and **c** model convective precipitation. The mean seasonal cycle (red line) and its standard deviation (blue shading) are shown

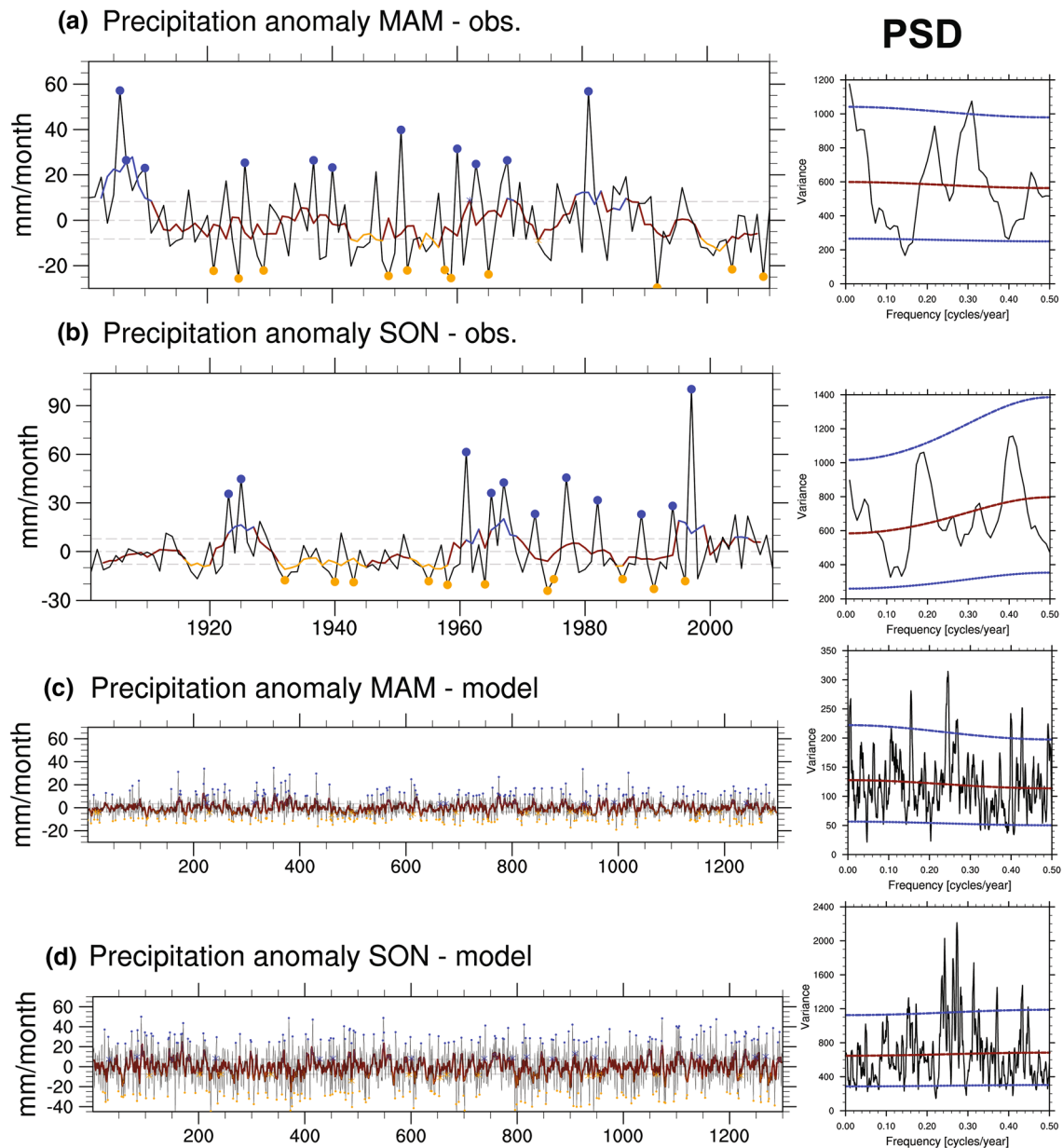


**Fig. 3** Seasonal precipitation (mm/month) anomaly time-series averaged over East Africa, along with power spectral density (PSD) plot for, **a, c** MAM and **b, d** SON seasons in **(a, b)** observations and **c, d** model convective precipitation. In the time-series, *red lines* indicate a 5-year running mean and blue (*orange*) dots indicate years identi-

fied as extreme wet (dry), and blue (*orange*) lines pluvial and drought periods. *Gray dashed horizontal lines* indicate the zero line and  $\pm 1$  standard deviations. PSD plots show variance for the dominant cycles, with the *blue lines* indicating a 95% confidence level according to a theoretical Markov spectrum

over the length of record. In addition, we also define sustained periods of above- and below-average MAM and SON rainfall, respectively. Such multi-year drought or pluvial periods are defined on the 5-year running mean of the time-series. A drought or pluvial is defined to occur when the running mean exceeds a cutoff value of  $\pm 1$  standard deviation. The starting point of a drought/pluvial was taken as the year when the running mean crossed the threshold of

$\pm 0.5$  standard deviation prior to the point of exceeding the cutoff value of  $\pm 1$  standard deviation. The endpoint of the drought/pluvial occurred when the running mean no longer exceeds the cutoff value of  $\pm 1$  standard deviation. In addition to incorporating the extreme conditions at the height of a drought or pluvial, this definition also includes the years leading *into* it. The approach chosen here follows Ummenhofer et al. (2011).

Extreme dry MAM seasons in the Horn of Africa region are all characterised by a rainfall deficit exceeding  $-20$  mm/month, with 1992 being the driest year with a deficit of  $-30$  mm/month (Fig. 3a). Dry MAM seasons occurred primarily during the 1920s, the late 1940s to early 1960s, and since the 2000s. Prolonged MAM drought conditions were observed during the 1940s and 1950s, and more recently in the 2000s, consistent with Nicholson et al. (2012). In contrast, the Horn experienced anomalously wet long rains at the start of the 20th century, with many extreme wet MAM seasons falling into those periods, as well as prolonged pluvial conditions (Fig. 3a). For the SON season, increasingly wetter short rains since the 1960s are apparent in the observations, consistent with Liebmann et al. (2014), with the majority of extreme SON seasons occurring post-1960 (Fig. 3b). With a rainfall anomaly in excess of 100 mm/month, 1997 experienced the wettest SON seen in the record. It was a strong El Niño event with concurrent positive IOD conditions in the Indian Ocean (Saji et al. 1999; Webster et al. 1999), resulting in widespread flooding across East Africa (e.g., Birkett et al. 1999). Prolonged drought conditions for the SON season occurred in the 1930s to the 1950s, consistent with the MAM season and Nicholson et al. (2012). From Fig. 3a,b it is also apparent that the magnitude of the rainfall anomalies during extreme wet years is considerably larger than during the extreme dry years. On the other hand, during the 20th Century, it appears that prolonged drought conditions are more persistent than pluvial conditions. It has to be noted, though, that the length of the observational record is limited and non-stationarity in the climate system needs to be kept in mind in this regard.

It is therefore of interest to assess extreme dry and wet conditions, as well as prolonged drought and pluvial periods in an extended record. The corresponding precipitation time-series for the Horn of Africa region over the 1300 years in the CESM simulation is therefore shown in Fig. 3c,d. The extended record provides considerably larger sample size of extreme dry/wet years, as well as more realisations of prolonged drought/pluvial conditions. The asymmetry in the magnitude of the rainfall anomalies between extreme dry and wet years in the observations is less pronounced in the model: minimum and maximum values in the model vary from  $-19$  to 35 mm/month for MAM and  $-49$  to 50 mm/month for SON. Prolonged drought conditions, incurred for 263 MAM (272 SON) seasons over the length of record, compared to 261 pluvial MAM (268 SON) seasons, are also readily apparent.

A power spectral density (PSD) analysis of the MAM precipitation time-series reveals a dominant period of 3–4 and 50 years in the observations, significant at the 95% level (Fig. 3a), while a peak at approximately 5 years in SON is not significant (Fig. 3b). In the model, significant

peaks for MAM occur around 4 and 6 years, as well as at multi-decadal to centennial frequency (Fig. 3c). For SON, a broad peak in the 3–4 year range and at 6 years is apparent (Fig. 3d). Peaks in the 3–6 year range are most likely associated with the well-known influence of ENSO on East African precipitation (e.g., Janowiak 1988; Ogallo 1988; Mutai et al. 1998; Indeje et al. 2000; Lyon and DeWitt 2012). In addition, the model also has significant peaks in East African precipitation at 33, 10, 6, and 2–3 years. The latter might reflect overly frequent ENSO events, though this model bias has been much improved in the latest version used here (cf. Richter and Rasch 2008, and references therein).

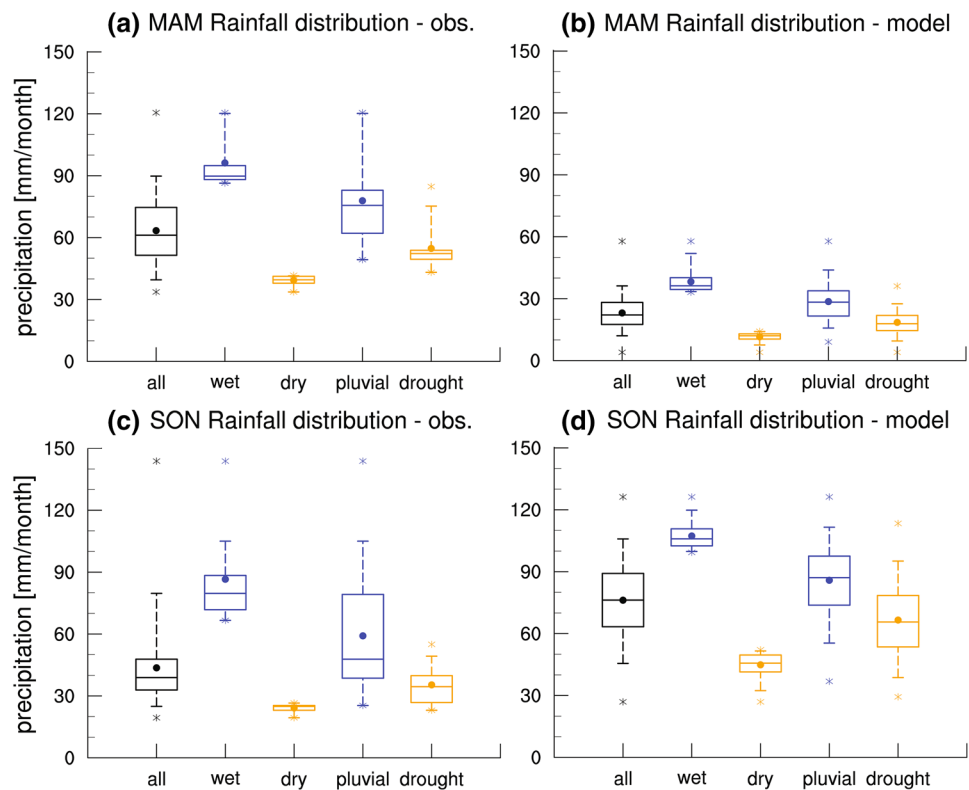
The distributions of rainfall during dry/wet and drought/pluvial seasons for the long and short rains for MAM and SON in the observations and model are further detailed in Fig. 4. In the observations, the extreme dry (wet) MAM seasons recorded a median seasonal rainfall of 40 mm/month (90 mm/month), compared to 52 mm/month (76 mm/month) for the drought (pluvial) conditions (Fig. 4a). In contrast in the model, extreme dry (wet) median rainfall during MAM were 12 mm/month (36 mm/month), while droughts (pluvials) were characterised by a median seasonal MAM rainfall of 18 mm/month (28 mm/month; Fig. 4b). As such, dry and wet extremes during MAM in the observations differed by a factor of  $\sim 2$  and a factor of  $\sim 3$  in the model. While the model consistently underestimates MAM rainfall, the variability across dry/wet extremes and droughts/pluvials is better represented. Dry extremes and droughts do not feature a large interquartile range, while wet extremes and pluvials do (Fig. 4a, b). This is seen in both the observations and model and is consistent with larger rainfall deviations during wet compared to dry conditions (cf. Fig. 3).

For the short rains, dry (wet) extreme SON seasons recorded 25 mm/month (80 mm/month) in the observations, compared to 46 mm/month (76 mm/month) in the model, with the latter consistently wetter than the observations (Fig. 4c, d). Similarly, SON median rainfall during pluvial (drought) conditions was 48 mm/month (34 mm/month) in the observations compared to 87 mm/month (66 mm/month) for the model. Again, the range in the rainfall amounts during wet extremes and pluvials for SON is larger than for dry extremes and droughts.

We further explore the characteristics of dry/wet and drought/pluvial years in the Horn of Africa region in Fig. 5, which shows the seasonal cycle of precipitation in the observations and model during the years when the MAM and SON seasons, respectively, were classified as extreme in Fig. 3. To assess whether the seasonal cycle during seasons with extreme hydroclimatic conditions deviates significantly from average conditions, we used a Monte Carlo test (cf. Ummenhofer et al. 2011): for each category (dry/



**Fig. 4** Boxplot of seasonal precipitation (mm/month) over East Africa for **a, b** MAM and **c, d** SON seasons for **a, c** observations and **b, d** model convective precipitation for all years (*black*) and years identified as dry/drought (*orange*) and wet/pluvial (*blue*) in Fig. 3. The horizontal lines of the box indicate the 75% quantile, median, and 25% quantile, while the whiskers the 95% and 5%, stars maximum and minimum values, and the solid dot the mean



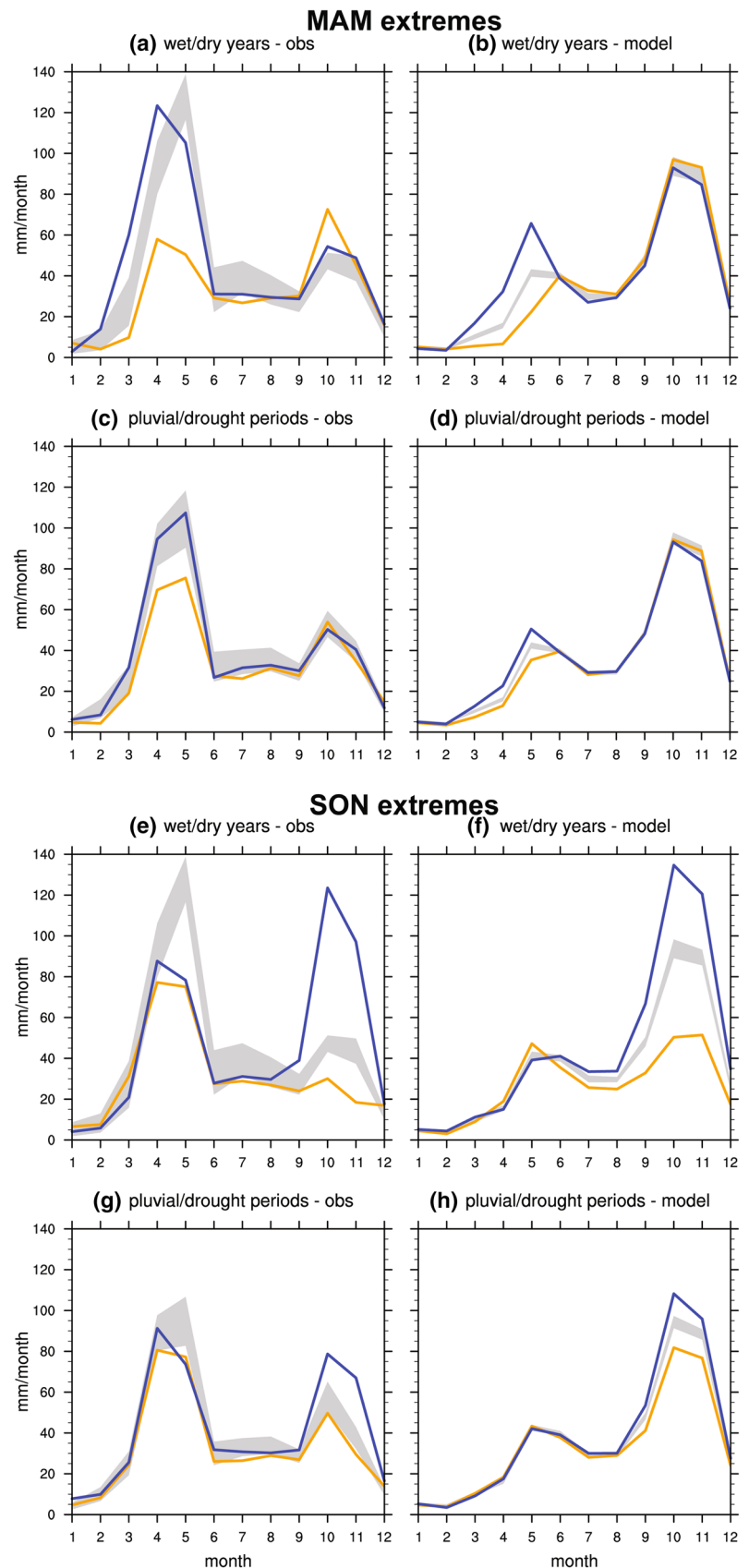
wet/drought/pluvial),  $n$  represents the number of years falling into this category. We randomly picked  $n$  years and determined their mean seasonal cycle for each category. This was repeated 10,000 times to produce a probability density distribution of expected precipitation by month for a given  $n$ . The gray shading in Fig. 5 represents the lower and upper bounds of a 90% confidence interval for the randomly generated distribution. Where the blue/orange lines lie outside the gray shading, the precipitation differs significantly from average seasonal conditions.

For the MAM season, extreme dry/wet seasons were characterised by significantly reduced/enhanced rainfall during these months for both the observations and model (Fig. 5a, b). In contrast, rainfall conditions returned to average for the remainder of the year (with the exception of dry MAM seasons recording above-average rainfall during the short rains in the observations). Similarly, drought and pluvial periods during MAM also experienced significant dry and wet deviations from average conditions only during the MAM season in the observations and model, but not during the rest of the year (Fig. 5c, d). Extremes during the SON season, on the other hand, exhibited large deviations in the rainfall not only during SON, but earlier in the year as well for both observations and model (Fig. 5e, f): dry SON seasons also recorded significant dry conditions during April–May and July in the observations and for

June–December in the model, while wet SON extremes in the model already exhibited significantly wetter conditions from July onwards. For drought and pluvial conditions, drier conditions early in the year only occurred for observed SON droughts, with rainfall anomalies otherwise more restricted to the SON season (Fig. 5g, h).

It is apparent that an asymmetry exists in regard to the seasonality of rainfall anomalies depending on the timescale under consideration: For the MAM season, the deviations in rainfall are restricted mostly to the long rain season only, irrespective of the timescale. However, dry (wet) SON seasons are characterised by a considerable decrease (increase) throughout most of the year (Fig. 5e, f); in contrast, prolonged drought/pluvial SON seasons record reduced/enhanced precipitation only during the short rains, respectively (Fig. 5g, h). Such nonlinearity in precipitation conditions with regard to timescale is crucial for understanding variations in East African climate and hints at differing mechanisms responsible for anomalous hydroclimatic conditions in the region on interannual and decadal timescales, as well as for drought and pluvial conditions, as suggested by Nicholson (2015). In the model, there is a bias to underestimate the long rains and overestimate the short rains, potentially linked to biases in the Turkana jet as discussed before. Despite this, as in observations, dry/wet SON seasons in the

**Fig. 5** Seasonal cycle in precipitation (mm/month) over East Africa for, **a–d** MAM and **e–h** SON extremes for (*left*) observations and (*right*) model convective precipitation. *Gray shading* indicates the average seasonal cycle, while *orange* and *blue lines* represent the mean seasonal cycle during *n* years identified as (*top*) dry and wet or (*bottom*) drought and pluvial. Where the *orange/blue lines* lie outside the *gray shading*, the values are significantly different from the long-term seasonal cycle at the 90% confidence level (according to Monte Carlo testing)



model are also associated with significantly lower/higher precipitation throughout much of the year, including both long and short rains, compared to conditions only being anomalous during the short rains during drought/pluvial

periods. In the following, we thus explore how the dry/wet and drought/pluvial conditions in the Horn of Africa relate to broader Indo-Pacific climatic anomalies in the observations and model.

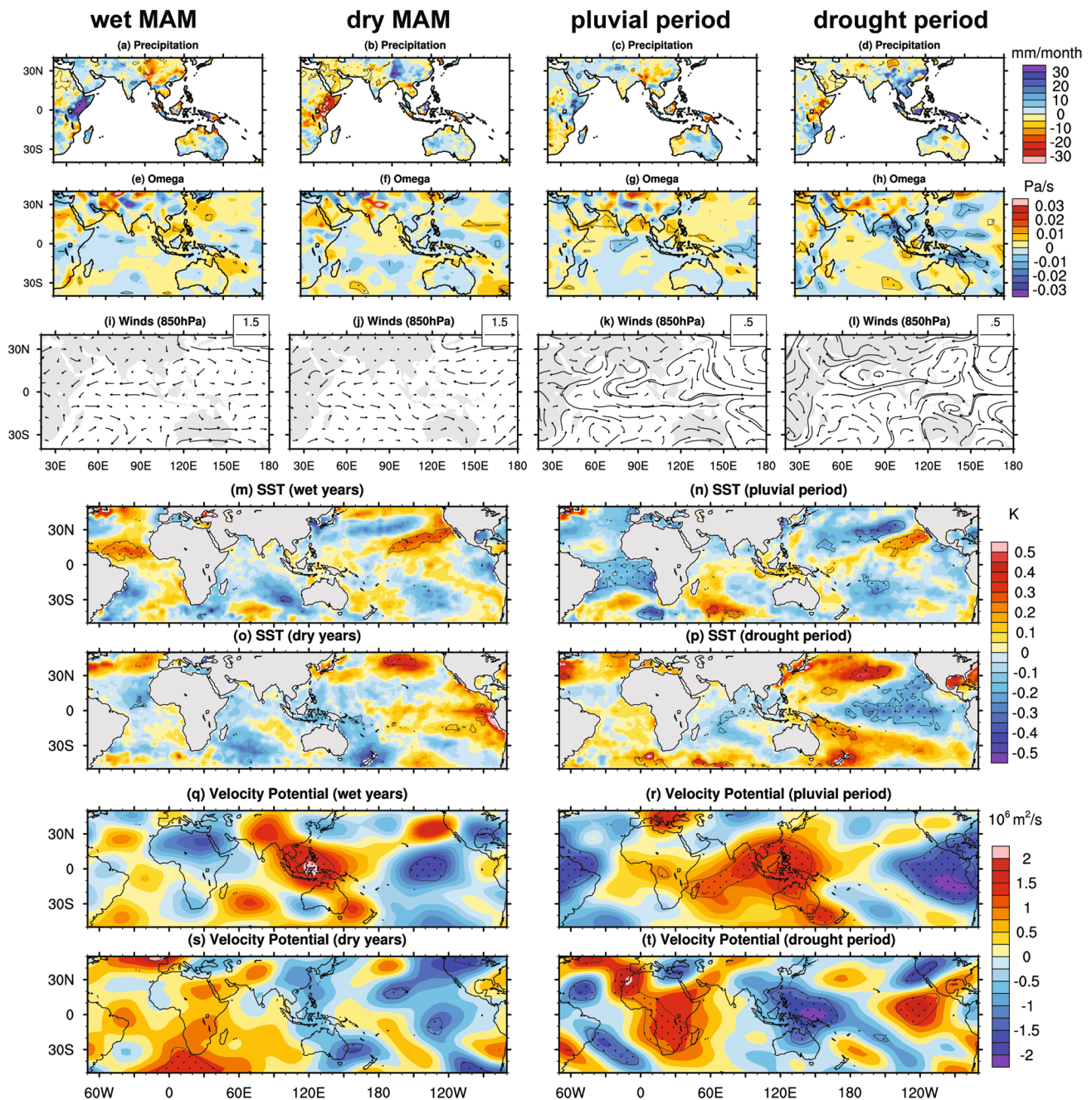


**Fig. 6** Observed MAM composite climate anomalies during extreme MAM hydroclimate conditions in East Africa as identified in Fig. 3a for, **a–d** precipitation (mm/month), **e–h** vertical velocity  $\Omega$  (Pa/s), **i–l** winds at the 850hPa level (m/s), **(m–p)** SST (K), and **(q–t)** velocity

potential at the 200 hPa level ( $10^6 \text{ m}^2/\text{s}$ ). *Stippling* and *red* vectors indicate anomalies that are significant at the 95% level according to a two-tailed *t*-test

## 4 Links between East African hydroclimatic extremes and Indo-Pacific climate anomalies

### 4.1 Indo-Pacific climate anomalies for extreme hydroclimatic conditions—MAM

The climate anomalies for MAM during extreme hydroclimatic conditions are given for observations in Fig. 6. Years with enhanced East African long rains (+20 mm/month) are characterised by drier conditions across the eastern Indian Ocean, including the Maritime Continent and western Australia during MAM (Fig. 6a). These rainfall patterns are consistent with anomalous descent over the IPWP and ascent over East Africa, as seen in the 700hPa  $\Omega$  field and the 200hPa velocity potential (Fig. 6e, q). The latter reflects large-scale vertical motions associated with shifts in the Walker circulation. Low-level wind convergence over the East African coast and divergent anomalies over the Maritime Continent are also seen (Fig. 6i). Significant warm SST anomalies occur over the tropical Atlantic and the subtropical North Pacific (10°–25°N; Fig. 6m). The Indian Ocean is characterised by cool SST, albeit mostly not significant, apart from locally in the southeast Indian Ocean.

Years characterised by dry conditions over East Africa (−20 mm/month) also record reduced rainfall over the southern Arabian Peninsula and the northern Indian subcontinent (Fig. 6b). The unusually dry regions are subject to large-scale descending motion over the broader Indian region, while there is anomalous ascent over the IPWP (Fig. 6f, s). Dry years in East Africa are also characterised by warm SST across the eastern equatorial Pacific reminiscent of El Niño conditions (Fig. 6o).

The precipitation patterns for East African pluvial and drought periods exhibit similar features to dry and wet years, but the anomalies are of reduced magnitude (Fig. 6c, d). A pronounced positive anomaly in 200hPa velocity potential is seen over the IPWP region and adjacent land areas and extending towards the southeast to Madagascar during pluvial episodes in the observations (Fig. 6r). In contrast, prolonged drought episodes during MAM are associated with La Niña-type SST anomalies in the Pacific and cool SST in the central Indian Ocean. The 200hPa velocity potential indicates significant negative anomalies over the IPWP region and anomalous descending motion over the African continent (Fig. 6t). Overall, the composite anomalies between dry/wet extremes and drought/pluvial episodes are broadly similar for MAM for the observations (Fig. 6). A striking exception is the Pacific SST anomaly pattern during MAM dry extremes and drought episodes, resembling El Niño and La Niña conditions, respectively (Fig. 6m–p).

Similar to the observations, East African wet years in the model are also characterised by significantly more MAM precipitation over the Arabian Peninsula and into

the Indian subcontinent (Fig. 7a) in line with anomalous ascent over these regions (Fig. 7e, q). The equatorial Indian Ocean exhibits easterly wind anomalies at the 850hPa level and convergence over coastal East Africa during MAM (Fig. 7i). Enhanced southwesterly onshore flow over the Indian subcontinent accounts for wetter conditions there. Anomalous cool SST anomalies are seen in the tropical Atlantic and Pacific, the latter reminiscent of La Niña conditions, while the northern Indian Ocean is anomalously warm and the southern Indian Ocean cool (Fig. 7m). The simulated precipitation pattern for dry years is broadly consistent with the pattern in observations, with dry conditions over East Africa and into the Arabian Peninsula and the Indian subcontinent (Fig. 7b). Regions of anomalous ascent/descent during dry years are consistent with the rainfall pattern and opposite to those seen during the extreme wet years (Fig. 7f).

The large-scale atmospheric circulation during wet years in East Africa indicates a shift in the Walker circulation with broadscale descending motion over the eastern and central equatorial Pacific seen in the 200hPa velocity potential (Fig. 7q) and associated with cool SST anomalies there (Fig. 7m). In contrast, anomalous ascent occurs over the western Indian Ocean with warm SST, including over India, the Arabian Peninsula, and East Africa (Fig. 7m, q). The SST and large-scale Walker circulation anomalies during dry years in East Africa are reversed (Fig. 7o, s). Overall, extreme dry and wet years in East Africa in the model during MAM exhibit anomalies of opposite sign. As such, the anomaly patterns are relatively symmetric with regard to sign, unlike the signals in observations which are much less linear during dry and wet years.

The modeled precipitation anomaly pattern for pluvial and drought periods is similar to dry and wet extremes during MAM (Fig. 7c, d). Interestingly, the significant SST anomalies in the Pacific shift from the eastern Pacific for extreme dry and wet seasons to the western Pacific for drought and pluvial periods in the model (Fig. 7m–p). Consistent with this, significant velocity potential anomalies of opposite sign are also located more over the western Pacific and centred over the East African region for prolonged hydroclimatic conditions. Williams and Funk (2011) previously suggested that a westward shift in the Walker circulation over the IPWP contributed to the reduced East African long rains during the March–June months in recent decades.



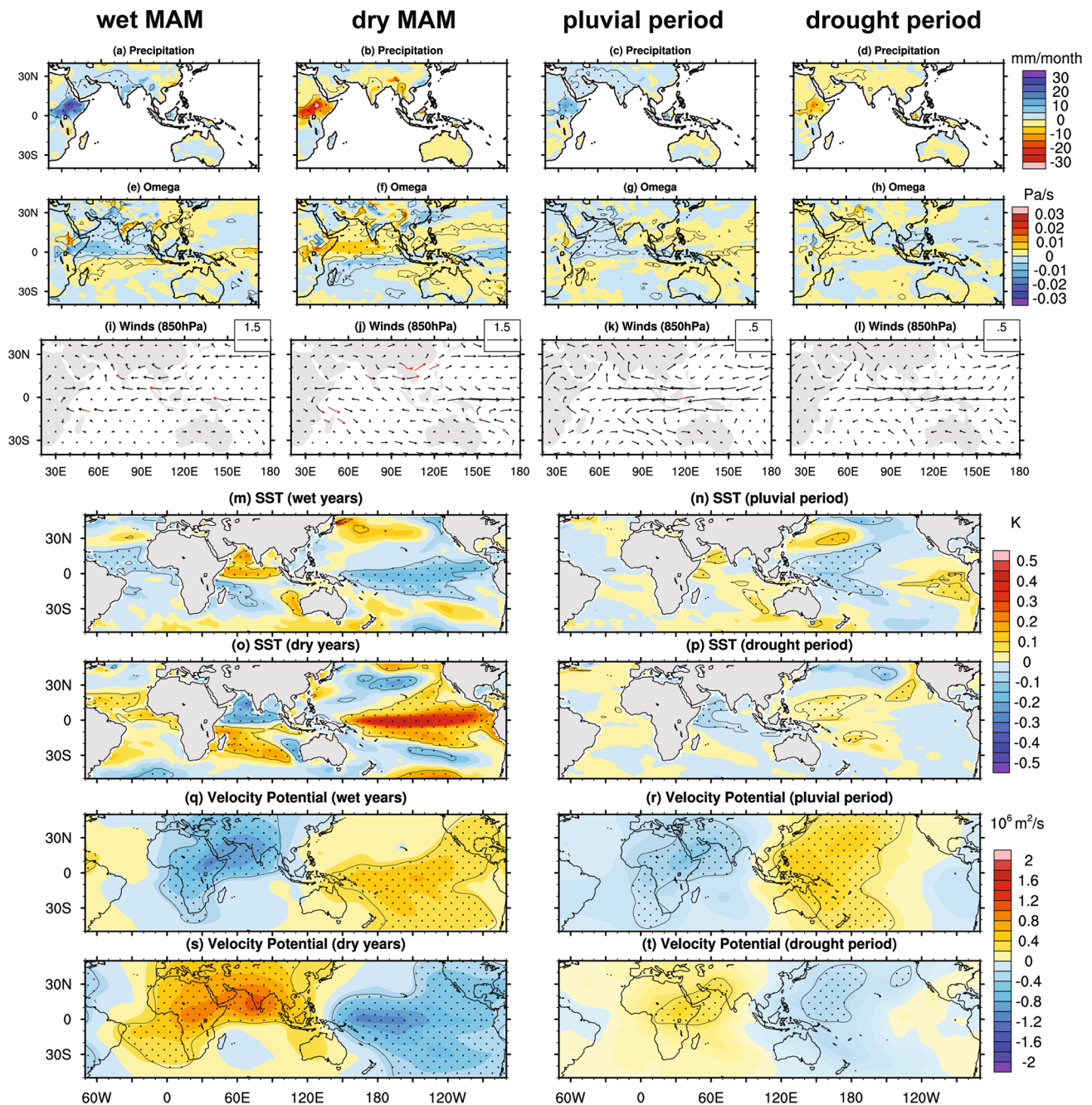


**Fig. 7** Model MAM composite climate anomalies during extreme MAM hydroclimate conditions in East Africa as identified in Fig. 3b for, **a–d** precipitation (mm/month), **e–h** vertical velocity  $\Omega$  (Pa/s), **i–l** winds at the 850 hPa (m/s), **m–p** SST (K), and **q–t** velocity poten-

tial at the 200 hPa level ( $10^6 \text{ m}^2/\text{s}$ ). Stippling and red vectors indicate anomalies that are significant at the 95% level according to a two-tailed *t*-test

#### 4.2 Indo-Pacific climate anomalies for extreme hydroclimatic conditions—SON

During the short rain season, East African wet years in observations are characterised by dry conditions over the Maritime Continent and much of Australia (Fig. 8a). The rainfall anomalies are associated with anomalous descent

over the Maritime Continent region, while ascending anomalies occur over the western Indian Ocean and African continent (Fig. 8e, q). Easterly low-level winds across the tropical Indian Ocean are enhanced during SON (Fig. 8i). The Indo-Pacific SST anomalies are reminiscent of a positive IOD and El Niño event, with cool SST in the eastern Indian Ocean, warm in the west, and warm SST

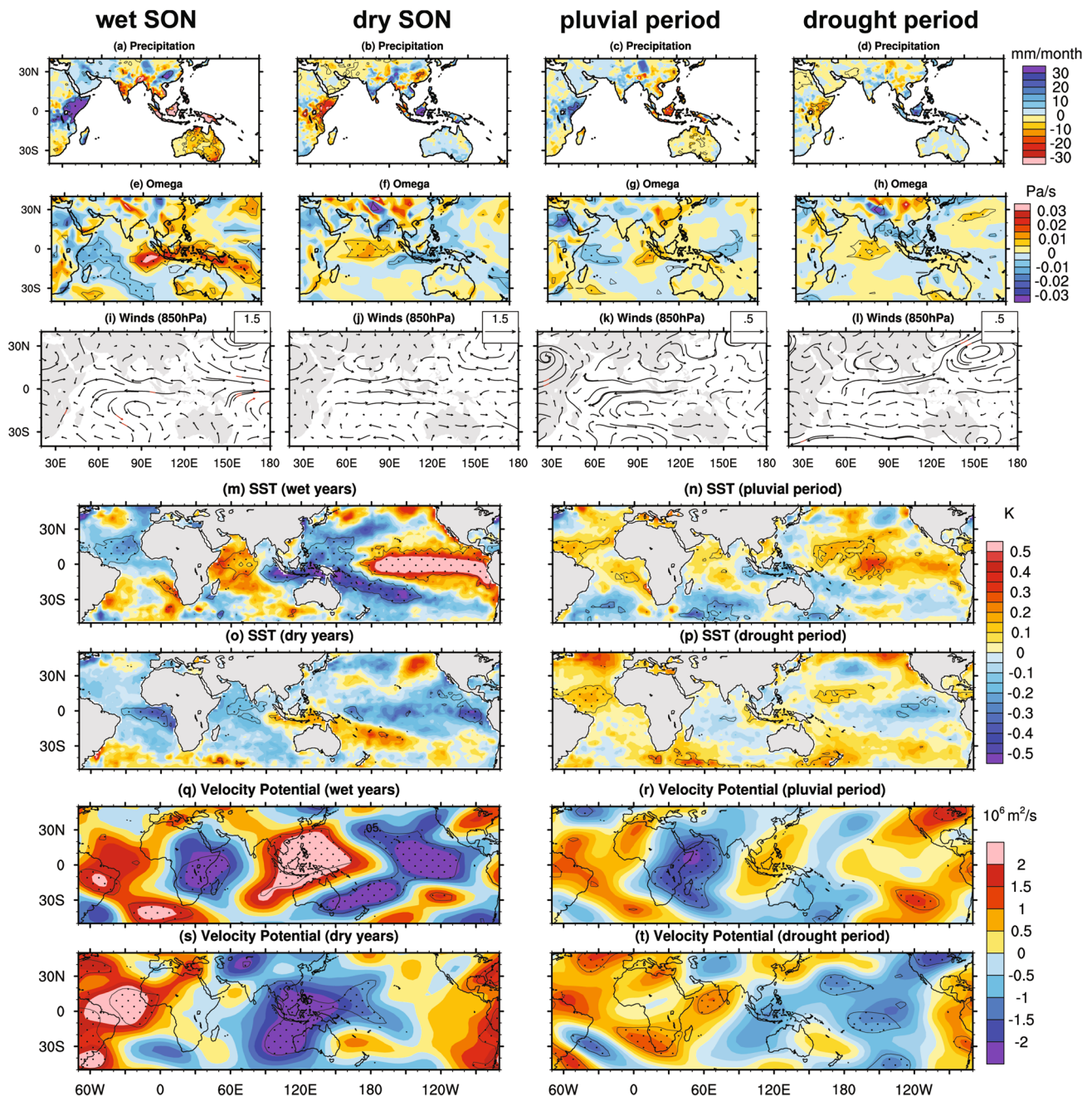


**Fig. 8** As Fig. 6, but for the SON months

anomalies in excess of 0.5K across the eastern and central equatorial Pacific (Fig. 8m). This is consistent with more variable and wetter short rains with a warmer western Indian Ocean (Liebmann et al. 2014), a strengthening of the Walker cell over the Indian Ocean (Nicholson 2015), and a strengthening of the IOD-East African rainfall relationship in recent decades (Manatsa and Behera 2013).

In contrast dry East African years during SON exhibit cool SST over the Indian Ocean and in the equatorial

Pacific reminiscent of La Niña conditions (Fig. 8o). Changes in the zonal circulation over the Indian Ocean region and adjacent land areas include westerly low-level winds over the eastern Indian Ocean, accounting for wet conditions over the Maritime Continent (Fig. 8b, j). Drought and pluvial years in East Africa exhibit patterns of Indo-Pacific climate anomalies during SON broadly consistent with those during extreme dry/wet years (Fig. 8). However, the magnitude of and area of significance for the



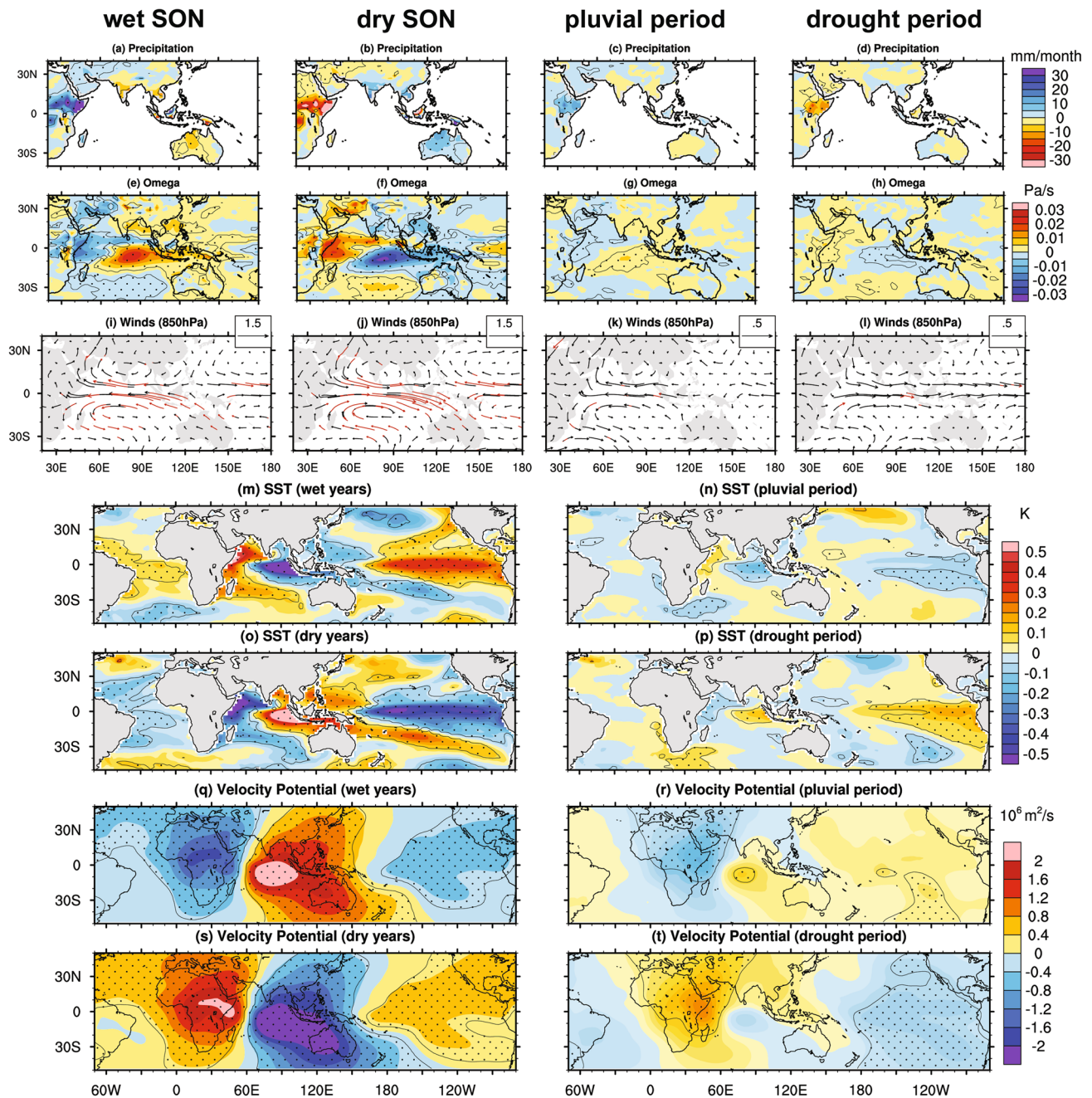


**Fig. 9** As Fig. 7, but for the SON months

anomalies is considerably reduced for the lower-frequency extremes in the observations. This is likely due to the fact that the number of years in the drought and pluvial periods is small, owing to the short observational record.

In the model, wet years in East Africa are characterised by enhanced rainfall over East Africa and the Arabian Peninsula, while the Maritime Continent and western half of Australia experience dry conditions (Fig. 9a). The rainfall patterns are associated with extensive

ascending anomalies over the western Indian Ocean and adjacent land areas, while the eastern Indian Ocean and IPWP region are characterised by descending motion, as seen in both the  $\Omega$  field at 700hPa and velocity potential at 200hPa (Fig. 9e, q). Significant easterly flow anomalies occur across the equatorial Indian Ocean and extending into East Africa (Fig. 9l). The SST during wet years in East Africa exhibit features of an El Niño event in the Pacific, with significant warm SST in the central and

eastern equatorial Pacific in excess of 0.5K. In addition, positive IOD conditions occur in the Indian Ocean, with anomalous cool SST in the eastern Indian Ocean off Java and Sumatra and warm in the west, and warm SST in the tropical Atlantic (Fig. 9m). The situation during dry years in East Africa is reversed during SON (Fig. 9).

During pluvial and drought years in East Africa in the model, significant rainfall anomalies during SON are restricted to East Africa only (Fig. 9c, d). Significant SST anomalies are reduced in magnitude overall. However, SST conditions in the Indian Ocean are still reminiscent of positive and negative IOD events for pluvial and drought periods, respectively, and associated with anomalous ascent/descent over the East African region (Fig. 9n, p, r, t). For East African prolonged hydroclimatic extremes, significant anomalies in SST, vertical velocities at 700hPa or 200hPa velocity potential over the Atlantic have disappeared, while they are very much reduced in magnitude and spatial extent over the tropical Pacific, especially for pluvial periods, compared to wet/dry years.

## 5 Low-frequency variability in the Indian and Pacific Oceans

It is of interest to further investigate Indo-Pacific variability in relation to timescale, given that there are indications that interannual to decadal East African precipitation anomalies seem to be associated with significant SST anomalies in the Pacific and Indian Ocean basins, respectively. Figure 10 shows the correlation between East African precipitation and SST, both unfiltered and band-pass filtered (10–20 years), for MAM and SON in the model. It is apparent that at interannual timescales, East African precipitation during both MAM and SON is highly correlated to tropical SST in all the ocean basins, in particular across the Indian and Pacific Ocean (Fig. 10a, c). On decadal timescales, however, significant correlations between East African precipitation and SST are limited to the western Indian Ocean, the eastern Indian Ocean and IPWP area, as well as the Pacific, reminiscent of the extratropical component of the Interdecadal Pacific Oscillation (IPO) pattern. No significant correlations to the eastern Pacific are apparent on these longer timescales (Fig. 10b, d).

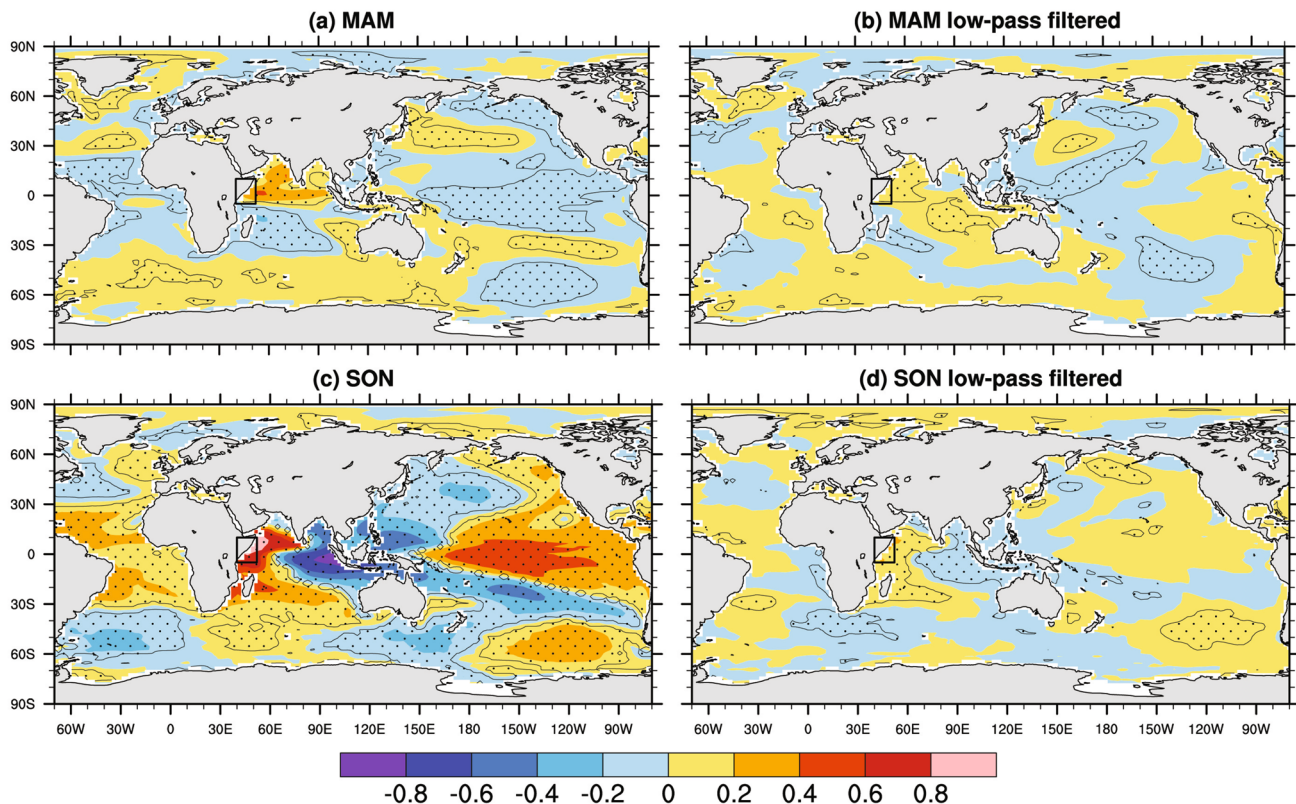


**Fig. 10** Correlation between model East African precipitation and SST are shown for, **a, c** raw and **b, d** low-pass filtered data for the **a, b** MAM and **c, d** SON seasons. A Butterworth bandpass filter was

used with a high- and low-pass frequency cutoff of 10 and 20 years, respectively. Stippling indicates significant correlations at the 95% confidence level



It should be noted that the correlations between East African precipitation and Indo-Pacific SST (Fig. 10a, c) are overly strong in the model, compared to observations especially in MAM (figure not shown). This is consistent with results in Fig. 1e–h, namely that the correlation between the DMI and Niño3.4 index and precipitation over the Horn of Africa region is overestimated in the model. It suggests that the model over-emphasises the interannual variance, compared to observations, likely due to an unrealistically strong ENSO-teleconnection (cf. Fig. 1e–f). This could be consistent with other CMIP5 models, as shown by Funk and Hoell (2015) when decomposing Indo-Pacific SST into a component associated with ENSO and a trend mode with strong warming in the western Pacific and IPWP area since the 1990s. While the trend mode in the CMIP5 models is consistent with observations and associated with significant drying in parts of East Africa, the ENSO mode exhibits too much warming in the eastern Pacific (Funk and Hoell, 2015). East African precipitation responses to Indo-Pacific (multi-)decadal variability, such as that associated with the recent warming hiatus (e.g., Kosaka and Xie 2013; England et al. 2014), might thus not be captured well due to the

model underestimating Indo-Pacific variability at low frequencies compared to ENSO-related interannual variability.

Furthermore, a gridpoint-by-gridpoint PSD analysis is performed on SST in the observations for the period 1870–2010 and the 1300-year model simulation. The resultant longest significant period for each gridpoint is shown in Fig. 11 for the MAM and SON season. In the observations, the tropical Pacific Ocean is characterised by strong subdecadal variability, while the North Pacific, North Atlantic, Indian Ocean, and large parts of the Southern Ocean exhibit low-frequency variability on timescales of 30 years and longer (Fig. 11a, c). The broad features of dominant frequencies are consistent for the MAM and SON season, with the following exceptions: the western South Pacific during SON exhibits variability on the 16–24 year timescale compared to shorter sub-decadal variability in MAM; the eastern Indian Ocean off Java and Sumatra in proximity to the eastern pole of the IOD is characterised by low-frequency variability on timescales of 30 years and longer during MAM, but shows variability in the 10–20 year range during SON (Fig. 11a, c). However, limitations in data availability and the short length of record pose

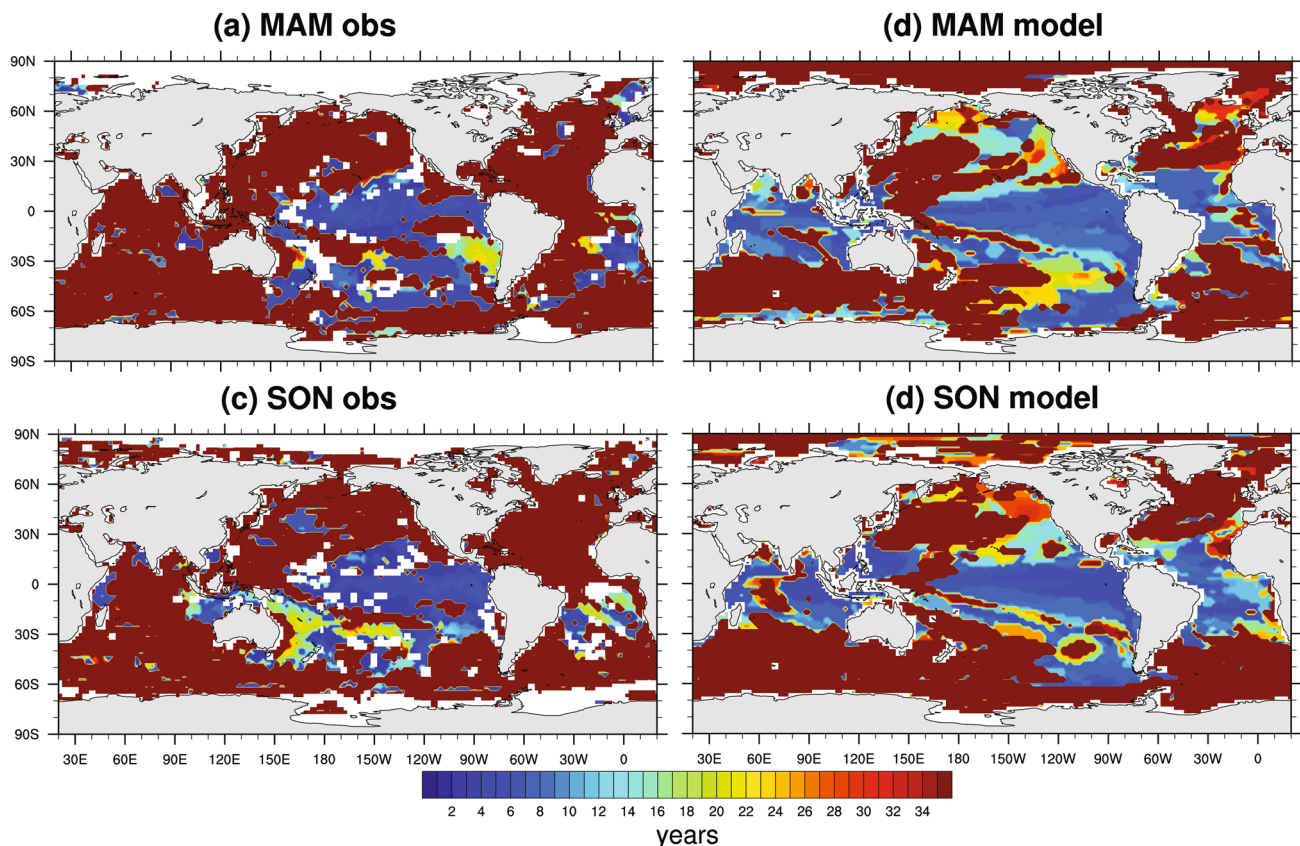


**Fig. 11** Longest dominant period of SST variance (in years) for, **a**, **c** observed and **b**, **d** model for the **a**, **b** MAM and **c**, **d** SON season, respectively, based on power spectral density analysis of SST at each

gridpoint to determine where the 90% (95%) confidence level according to a theoretical Markov spectrum is exceeded for the observations (model)

challenges for this analysis using observationally-based products, as some of the results could be artifacts of the interpolation methods used in data-sparse regions.

In the 1300-year model simulation, clear spatial variation in the low-frequency signal is also apparent, varying from interannual in the tropical regions of the three ocean basins to multi-decadal on timescales longer than 35 years for much of the Southern Ocean, North Atlantic and Arctic Ocean (Fig. 11b, d), consistent with Monselesan et al. (2015). In the Pacific, the longest significant periods in the eastern equatorial region in particular do not exceed 10 years, while the subtropical gyres exhibit lower-frequency variability on decadal to multi-decadal timescales. Such low-frequency variability is also seen in the equatorial central-western Pacific (130°–160°E, 10°S–10°N). The Indian Ocean north of 30°S in the model is characterised for the most part also by variability not exceeding 10 years. However, the central and northern Indian Ocean locally exhibit variability with longer periods in excess of 25 years, in particular during SON (Fig. 11d). This pattern is consistent with Tozuka et al. (2007), who showed that the leading EOF of low-pass filtered SST, which explained 37% of decadal variability in their 200-year SINTEX-F1 simulation, had enhanced loading in the northern and western Indian Ocean, while the eastern equatorial Indian Ocean exhibited less low-frequency variability. This is also consistent with findings by Tierney et al. (2013).

Overall, Fig. 11 seems to suggest that while SST in the eastern equatorial Pacific are dominated by higher-frequency variability in the ENSO band (~4–7 years), the tropical Indian Ocean and western Pacific exhibits lower-frequency SST variability beyond 10 years. This could explain the different contribution to regional precipitation anomalies for the Pacific and Indian Ocean on interannual and decadal timescales, respectively, as shown here for East Africa (Figs. 6, 7, 8, 9; see also Tierney et al. (2013) or previously for Southeastern Australia (Ummenhofer et al. 2009a, 2011). In the model, the dominant low-frequency signal in the Indian Ocean is not well-represented and the model instead exhibits overly strong variability on the subdecadal timescale (Fig. 11b, d). This could be linked to overly strong coupling between ENSO and the IOD in the model, while the strength of the ENSO-IOD coupling relationship in observations has decreased in recent decades (Ham et al. 2016). Given the limited observational record, considerable uncertainty remains as to the strength of the low-frequency variability in observations in the Indian Ocean. However, underestimating the low-frequency variability in the Indian Ocean in the model, while at the same time overestimating the effect of ENSO on East African rainfall—either directly or through overly strong ENSO-IOD coupling (e.g., Ham

et al. 2016)—might account for the over-estimate of SON precipitation in the seasonal cycle compared to observations (Fig. 2). This feature is commonly encountered in present-generation climate models, which makes rainfall projections in the vulnerable Horn of Africa region problematic (Tierney et al. 2015).

## 6 Conclusions

Recent work demonstrated that current state-of-the-art climate models consistently overestimate the short rain season, while underestimating the long rains over the Horn of Africa (Yang et al. 2014; Tierney et al. 2015). This inability to represent the seasonal cycle makes it problematic for climate models to project changes in precipitation for East Africa. Here we explore whether this has also implications for interannual and decadal variability during the long and short rains in East Africa. To investigate these aspects in a consistent framework, we used an unforced multi-century CESM simulation to compare the role of Indo-Pacific variability on East African rainfall on interannual and decadal timescales.

Precipitation in the Horn of Africa in observations positively correlated with ENSO within 5° of the equator and along the coast, while negative anomalies were seen poleward of 10°N/S. Broad features of the ENSO-precipitation correlation were captured by the model, though the area of high correlations was much stronger and more restricted to the coast and southern Horn compared to the observations. East African precipitation also correlated positively with the IOD, though the correlation coefficient over the Horn region was overly strong in the model. It was also apparent that the magnitude of the rainfall anomalies during wet extremes was considerably larger than during the dry extremes, while in observations prolonged droughts were more persistent than pluvial conditions. It should be noted, though, that the length of the observational record is limited and considerable non-stationarity of the climatic drivers exists in the region (Nicholson 2015).

An asymmetry was apparent in regard to the seasonality of precipitation anomalies in observations depending on the timescale under consideration: For the MAM season, the deviations in rainfall are restricted mostly to the long rain season only, irrespective of the timescale. However, dry (wet) SON seasons are characterised by a considerable decrease (increase) throughout most of the year; in contrast, prolonged drought/pluvial SON seasons record reduced/enhanced precipitation only during the short rains, respectively. Such nonlinearity in precipitation conditions with regard to timescale is crucial for understanding variations in East African climate and hints at different mechanisms

responsible for anomalous hydroclimatic conditions in the region on interannual and decadal timescales.

We further explored how the dry/wet and drought/pluvial conditions in the Horn region related to broader Indo-Pacific climate anomalies in the observations and model during the long and short rain seasons. Interannual variations in East African hydroclimate coincided with significant Indo-Pacific SST anomalies, including those associated with ENSO, and linked to changes in the Walker circulation, regional winds and vertical velocities over East Africa in observations and the model. During dry/wet years in East Africa, Indo-Pacific climate anomalies reminiscent of ENSO were seen in the model during both MAM and SON, while this was only the case during SON in the observations. During East African pluvial and drought years, significant SST anomalies in the Indian Ocean, resembling positive and negative IOD events, respectively, appeared associated with anomalous ascent/descent over the East African region. For East African pluvial/drought years, significant anomalies in SST,  $\Omega$  field at 700hPa or 200hPa velocity potential over the Atlantic Ocean disappeared and were much reduced in the Pacific, compared to wet/dry years. Interestingly, for MAM the significant SST anomaly in the Pacific shifts from the eastern Pacific for extreme dry/wet seasons to the western Pacific for drought/pluvial periods in the model.

We thus compared the correlation between East African precipitation and SST for interannual and decadal timescales. It is apparent that at interannual timescales, East African precipitation during both MAM and SON is highly correlated to tropical SST in all the ocean basins, in particular across the Indian and Pacific Ocean. On decadal timescales, however, significant correlations between East African precipitation and SST are limited to the western Indian Ocean, the eastern Indian Ocean and IPWP area, as well as the Pacific, reminiscent of the extratropical component of the IPO pattern. No significant correlations to the eastern Pacific are apparent on these longer timescales.

Furthermore, dominant frequencies in Indo-Pacific SST were assessed: it was found that the tropical Pacific was characterised by strong subdecadal variability, while the North Pacific, North Atlantic, Indian Ocean and large parts of the Southern Ocean exhibited variability on timescales of 30 years and longer in observations. This broad pattern was consistent for MAM and SON, except for the eastern Indian Ocean off Java and Sumatra characterised by variability on timescales of 30 years during MAM, but showing variability in the 10–20 year range during SON. In the 1300-year simulation, the longest significant periods in the equatorial eastern Pacific did not exceed 10 years, while the subtropical gyres exhibited variability on decadal to multi-decadal timescales. The Indian Ocean in the model was characterised for the most part also by variability not

exceeding 10 years. However, the central and northern Indian Ocean locally exhibited variability with longer periods in excess of 25 years, in particular during SON. These results suggest that while SST in the eastern equatorial Pacific are dominated by higher-frequency variability in the ENSO band ( $\sim 4$ –7 years), the tropical Indian Ocean, in particular in the north and west, exhibits lower-frequency SST variability beyond 10 years. Underestimating the low-frequency variability in the Indian Ocean in the model, while at the same time overestimating the effect of ENSO on East African rainfall—either directly or through overly strong ENSO-IOD coupling (e.g., Ham et al. 2016)—might account for the over-estimate of SON precipitation in the seasonal cycle compared to observations. This feature is commonly encountered in present-generation climate models, which makes rainfall projections in the vulnerable Horn of Africa region problematic (Tierney et al. 2015).

**Acknowledgements** Use of the following data sets is gratefully acknowledged: Global Precipitation Climatology Center data set by the German Weather Service (DWD) through <http://gpcc.dwd.de>, NCEP/NCAR reanalysis data provided by NOAA/OAR/ESRL PSD, Boulder, Colorado, USA, through <http://www.cdc.noaa.gov>; Hadley Centre HadISST by the UK Met Office, and the Twentieth Century Reanalysis Project supported by the U.S. DOE, Office of Science Innovative and Novel Computational Impact on Theory and Experiment program, Office of Biological and Environmental Research, and NOAA Climate Program Office. We also gratefully acknowledge use of CESM output and thank NCAR for producing and making available their model output. Comments by two anonymous reviewers are gratefully acknowledged as they helped improve an earlier version of the manuscript. The project was supported by the U.S. National Science Foundation under OCE-1203892, C.C.U. also through the *Penzance* and *John P. Chase Memorial Endowed Funds*, and the *Investment in Science Fund* at WHOI, and M.K. through the Research Internships in Science and Engineering (RISE) program by the German Foreign Exchange Service.

## References

- Awange JL, Ferreira VG, Forootan E, Khandu SA, Andam-Akorful NO, Agutu He XF (2016) Uncertainties in remotely sensed precipitation data over Africa. *Int J Climatol* 36:303–323
- Awange JL, Forootan E, Kuhn M, Kusche J, Heck B (2014) Water storage changes and climate variability within the Nile Basin between 2002 and 2011. *Adv Water Resour* 73:1–15
- Bahaga TK, Tsidu GM, Kucharski F, Diro GT (2015) Potential predictability of the sea-surface temperature forced equatorial East African short rains interannual variability in the 20th century. *Quart J R Meteorol Soc* 686:16–26
- Behera SK, Luo J-J, Masson S, Delecluse P, Gualdi S, Navarra A, Yamagata T (2005) Paramount impact of the Indian Ocean Dipole on the East African short rains: A CGCM study. *J Clim* 18:4514–4530
- Birkett C, Murtugudde R, Allan R (1999) Indian Ocean climate event brings floods to East Africa's lakes and the Sudd Marsh. *Geophys Res Lett* 26(8):1031–1034



- Black E, Slingo J, Sperber KR (2003) An observational study of the relationship between excessively strong short rains in coastal East Africa and Indian Ocean SST. *Mon Weather Rev* 131:74–94
- Briegleb B, Bitz C, Hunke E, Lipscomb W, Holland M, Schramm J, Moritz R (2004) Scientific description of the sea ice component in the Community Climate System Model, version 3. Tech. rep., NCAR Technical Report No. NCAR/TN-463+STR
- Camberlin P, Okoola RE (2003) The onset and cessation of the “long rains” in eastern Africa and their interannual variability. *Theor Appl Climatol* 75:43–54
- Christensen JH et al (2013) Climate phenomena and their relevance for future regional climate change. *Climate Change 2013: The Physical Science Basis. Contribution of Working Group I to the Fifth Assessment Report of the Intergovernmental Panel on Climate Change*, Stocker TF, Qin D, G.-K. Plattner, M. Tignor, S. K. Allen, J. Boschung, A. Nauels, Y. Xia, V. Bex, and P. M. Midgley, Eds., Cambridge University Press, Cambridge, UK, 1217–1308
- Compo GP et al (2011) The twentieth century reanalysis project. *Quart J R Meteorol Soc* 137:1–28
- Conway DHCDR, and Persechino A (2007) GCM simulations of the Indian Ocean dipole influence on East African rainfall: Present and future. *Geophysical Research Letters* 34: doi:10.1029/2006GL027 597
- Cook KH, Vizzy EK (2013) Projected changes in East African rainy seasons. *J Clim* 26:5931–5948
- Dai A (2006) Precipitation characteristics in eighteen coupled climate models. *J Clim* 19:4605–4630
- Danabasoglu G, Bates SC, Briegleb BP, Jayne SR, Jochum M, Large WG, Peacock S, Yeager SG (2012) The CCSM4 ocean component. *J Clim* 25:1361–1389
- Danabasoglu G, Ferrari R, McWilliams JC (2008) Sensitivity of an ocean general circulation model to a parameterization of near-surface eddy fluxes. *J Clim* 21:1192–1208
- Danabasoglu G, Marshall J (2007) Effects of vertical variations of thickness diffusivity in an ocean general circulation model. *Ocean Model* 18:122–141
- England MH et al (2014) Recent intensification of wind-driven circulation in the Pacific and the ongoing warming hiatus. *Nat Clim Change* 4:222–227
- Fox-Kemper B et al (2011) Parameterization of mixed layer eddies. Part III: implementation and impact in global ocean climate simulations. *Ocean Model* 39:61–78
- Funk C, Dettinger MD, Michaelsen JC, Verdin JP, Brown ME, Barlow M, Hoell A (2008) Warming of the Indian Ocean threatens eastern and southern African food security but could be mitigated by agricultural development. *Proceedings of the National Academy of Sciences* 105, 11 081–11 086
- Funk C, Dettinger MD, Michaelsen JC, Verdin JP, Brown ME, Barlow M, Hoell A (2014) Predicting East African spring droughts using Pacific and Indian Ocean sea surface temperature indices. *Hydrol Earth Syst Sci* 18:4965–4978
- Funk C, Hoell A (2015) The leading mode of observed and CMIP5 ENSO-residual sea surface temperatures and associated changes in Indo-Pacific climate. *J Clim* 28:4309–4329
- Giannini A, Biasutti M, Held I, Sobel A (2008) A global perspective on African climate. *Clim Change* 90:359–383
- Goddard L, Graham NE (1999) Importance of the Indian Ocean for simulating rainfall anomalies over eastern and southern Africa. *Journal of Geophysical Research* 104 (D16):19 099–19 116
- Gregory D, Kershaw R, Inness PM (1997) Parametrization of momentum transport by convection. II: tests in single-column and general circulation models. *Quart J R Meteorol Soci* 123:1153–1183
- Ham Y-G, Choi J-Y, Kug J-S (2016) The weakening of the ENSO-Indian Ocean Dipole (IOD) coupling strength in recent decades. *Climate Dynamics*. doi:10.1007/s00382-016-3339-5
- Hastenrath S (2007) Circulation mechanisms of climate anomalies in East Africa and the equatorial Indian Ocean. *Dyn Atmos Oceans* 43:25–35
- Hastenrath S, Polzin D, Camberlin P (2004) Exploring the predictability of the ‘short rains’ at the coast of East Africa. *Int J Climatol* 24:1333–1343
- Hastenrath S, Polzin D, Mutai C (2010) Diagnosing the droughts and floods in equatorial East Africa, during boreal autumn 2005–08. *J Clim* 23:813–817
- Hastenrath S, Polzin D, Mutain C (2007) Diagnosing the 2005 drought in equatorial East Africa. *J Clim* 20:4628–4637
- Hoell A, Funk C (2014) Indo-Pacific sea surface temperature influences on failed consecutive rainy seasons over eastern Africa. *Clim Dyn* 43:1645–1660
- Hoell A, Hoerling M, Eischeid J, Quan W-X, Liebmann B (2017) Reconciling theories for human and natural attribution of recent East Africa drying. *J Clim* 30:1939–1957
- Indeje M, Semazzi FHM, Ogallo LJ (2000) ENSO signals in East African rainfall seasons. *Int J Climatol* 20:19–46
- Janowiak JE (1988) An investigation of interannual rainfall variability in Africa. *J Clim* 1:240–255
- Jochum M (2009) Impact of latitudinal variations in vertical diffusivity on climate simulations. *Journal of Geophysical Research* 114(C01010): doi:10.1029/2008JC005 030
- Jochum M, Potemra J (2008) Sensitivity of tropical rainfall to Banda Sea diffusivity in the community climate system model. *J Clim* 21:6445–6454
- Kalnay E et al (1996) The NCEP/NCAR 40-year reanalysis project. *Bull Am Meteorol Soc* 77:437–471
- Kistler R et al (2001) The NCEP-NCAR 50-year reanalysis: monthly means CD-rom and documentation. *Bull Am Meteorol Soc* 82:247–267
- Kosaka Y, Xie S-P (2013) Recent global-warming hiatus tied to equatorial Pacific surface cooling. *Nature* 501:403–407
- Latif M, Dommenges D, Dima M, Grötzner A (1999) The role of Indian Ocean sea surface temperature in forcing East African rainfall anomalies during December–January 1997/98. *J Clim* 12:3497–3504
- Liebmann B et al (2014) Understanding recent eastern Horn of Africa rainfall variability and change. *J Clim* 27:8630–8645
- Liebmann B et al (2017) Climatology and interannual variability of boreal spring wet season precipitation in the eastern Horn of Africa and implications for its recent decline. *J Clim* 30:3867–3886
- Lyon B (2014) Seasonal drought in the Greater Horn of Africa and its recent increase during the March–May long rains. *J Clim* 27:7953–7975
- Lyon B, DeWitt DG (2012) A recent and abrupt decline in the East African long rains. *Geophysical Research Letters* 39(L02702): doi:10.1029/2011GL050 337
- Manatsa D, Behera SK (2013) On the epochal strengthening in the relationship between rainfall of East Africa and IOD. *J Clim* 26:5655–5673
- Manatsa D, Chipindu B, Behera SK (2012) Shifts in IOD and their impacts on association with East African rainfall. *Theor Appl Climatol* 110:115–128
- Manatsa D, Morioka Y, Behera SK, Matarira CH, Yamagata T (2014) Impact of Mascarene High variability on the East African ‘short rains’. *Clim Dyn* 42:1259–1274
- Manatsa D, Mudavanhu C, Mushore TD, Mavhura E (2016) Linking major shifts in the East Africa ‘short rains’ to the Southern Annular Mode. *Int J Climatol* 36:1590–1599



- Monselesan DP, O'Kane TJ, Risbey JS, Church J (2015) Internal climate memory in observations and models. *Geophys Res Lett* 42:1232–1242
- Mutai CC, Ward MN, Colman W (1998) Towards the prediction of East Africa short rains based on sea surface temperature-atmosphere coupling. *Int J Climatol* 18:975–997
- Neale R, Richter J, Park S, Lauritzen P, Vavrus S, Rasch P, Zhang M (2013) The mean climate of the Community Atmosphere Model (CAM4) in forced sst and fully coupled experiments. *J Clim* 26:5150–5168
- Neale RB et al (2012) Description of the NCAR Community Atmosphere Model (CAM 5.0). Tech. rep., NCAR Technical Note, NCAR/TN-486+STR, p 289
- Nicholson SE (2014) A detailed look at the recent drought situation in the Greater Horn of Africa. *J Arid Environ* 103:71–79
- Nicholson SE (2015) Long-term variability of the East African “short rains” and its links to large-scale factors. *International Journal of Climatology*. doi:[10.1002/joc.4259](https://doi.org/10.1002/joc.4259)
- Nicholson SE (2016a) An analysis of recent rainfall conditions in eastern Africa. *Int J Climatol* 36:526–532
- Nicholson SE (2016b) The Turkana low-level jet: mean climatology and association with regional aridity. *Int J Climatol* 36:2598–2614
- Nicholson SE (2017) Climate and climatic variability of rainfall over Eastern Africa. *Reviews of Geophysics*. doi:[10.1002/2016RG000544](https://doi.org/10.1002/2016RG000544)
- Nicholson SE, Dezfuli AK, Klotter DA (2012) A two-century precipitation dataset for the continent of Africa. *Bull Am Meteorol Soc* 93:1219–1231
- Ogalllo LJ (1988) Relationships between seasonal rainfall in East Africa and the Southern Oscillation. *J Climatol* 8(1):31–43
- Omondi PA et al (2014) Changes in temperature and precipitation extremes in the Greater Horn of Africa region from 1961 to 2010. *Int J Climatol* 34:1262–1277
- Ongoma V, Chen H (2016) Temporal and spatial variability of temperature and precipitation over East Africa from 1951 to 2010. *Meteorology and Atmospheric Physics*. doi:[10.1007/s00703-016-0462-0](https://doi.org/10.1007/s00703-016-0462-0)
- Parhi P, Giannini A, Gentile P, Lall U (2016) Resolving contrasting regional rainfall responses to El Niño over tropical Africa. *J Clim* 29:1461–1476
- Rayner NA, Parker DE, Horton EB, Folland CK, Alexander LV, Rowell DP (2003) Global analyses of sst, sea ice and night marine air temperature since the late nineteenth century. *Journal of Geophysical Research* 108(4407): doi:[10.1029/2002JD002670](https://doi.org/10.1029/2002JD002670)
- Reason CJC, Allan RJ, Lindesay JA, Ansell TJ (2000) Enso and climatic signals across the Indian Ocean basin in the global context: Part i, interannual composite patterns. *Int J Climatol* 20:1285–1327
- Richter JH, Rasch PJ (2008) Effects of convective momentum transport on the atmospheric circulation in the Community Atmosphere Model, version 3. *J Clim* 21:1487–1499
- Rowell DP, Booth BB, Nicholson SE, Good P (2015) Reconciling past and future rainfall trends over East Africa. *J Clim* 28:9768–9788
- Saji NH, Goswami BN, Vinayachandran PN, Yamagata T (1999) A dipole mode in the tropical Indian Ocean. *Nature* 401:360–363
- Schneider U, Becker A, Finger P, Meyer-Christoffer A, Ziese M, Rudolf B (2013) GPCC's new land surface precipitation climatology based on quality-controlled in situ data and its role in quantifying the global water cycle. *Theoretical and Applied Climatology*. doi:[10.1007/s00704-013-0860-x](https://doi.org/10.1007/s00704-013-0860-x)
- Shongwe M, van Oldenborgh G, van den Hurk B, van Aalst M (2011) Projected changes in mean and extreme precipitation in Africa under global warming. Part II: East Africa. *J Clim* 24:3718–3733
- Smith R et al (2010) The Parallel Ocean Program (POP) reference manual, ocean component of the Community Climate System Model (CCSM). Tech. rep., Los Alamos National Laboratory Tech. Rep. LAUR-10-01853, [Available online at <http://www.cesm.ucar.edu/models/cesm1.0/pop2/doc/sci/POPRefManual.pdf>], p 141
- Tierney JE, Smerdon JE, Anchukaitis KJ, Seager R (2013) Multidecadal variability in East African hydroclimate controlled by the Indian Ocean. *Nature* 493:389–392
- Tierney JE, Ummenhofer CC, deMenocal PB (2015) Past and future rainfall in the Horn of Africa. *Sci Adv* 1(e1500):682
- Tozuka T, Luo J-J, Masson S, Yamagata T (2007) Decadal modulations of the Indian Ocean Dipole in the SINTEX-F1 coupled GCM. *J Clim* 20:2881–2894
- Ummenhofer CC, England MH, Meyers GA, McIntosh PC, Pook MJ, Risbey JS, Sen Gupta A, Taschetto AS (2009a) What causes Southeast Australia's worst droughts? *Geophysical Research Letters* 36(L04706): doi:[10.1029/2008GL036801](https://doi.org/10.1029/2008GL036801)
- Ummenhofer CC, Sen Gupta A, England MH, Reason CJC (2009b) Contributions of Indian Ocean sea surface temperatures to enhanced East African rainfall. *J Clim* 22:993–1013
- Ummenhofer CC et al (2011) Indian and Pacific Ocean influences on Southeast Australian drought and soil moisture. *J Clim* 24:1313–1336
- Vigaud N, Lyon B, Giannini A (2017) Sub-seasonal teleconnections between convection over the Indian Ocean, the East African long rains and tropical Pacific surface temperatures. *Int J Climatol* 37:1167–1180
- Vizy EK, Cook KH (2012) Mid-twenty-first-century changes in extreme events over northern and tropical Africa. *J Clim* 25:5748–5767
- Vrieling A, Meroni M, Mude AG, Chantarat S, Ummenhofer CC, de Bie CAJM (2016) Early assessment of seasonal forage availability for mitigating the impact of drought on East African pastoralists. *Rem Sens Environ* 174:44–55
- Webster PJ, Moore AM, Loschnigg JP, Leben RR (1999) Coupled ocean-atmosphere dynamics in the Indian Ocean during 1997–98. *Nature* 401:356–360
- Williams AP, Funk C (2011) A westward extension of the warm pool leads to a westward extension of the Walker circulation, drying eastern Africa. *Clim Dyn* 37:2417–2435
- Williams AP et al (2012) Recent summer precipitation trends in the Greater Horn of Africa and the emerging role of Indian Ocean sea surface temperature. *Clim Dyn* 39:2307–2328
- Yang W, Seager R, Cane MA, Lyon B (2014) The East African long rains in observations and models. *J Clim* 27:7185–7202
- Yang W, Seager R, Cane MA, Lyon B (2015) The annual cycle of East African precipitation. *J Clim* 28:2385–2404